Geophys. J. Int. (1995) **123**, 683–714

Bounds on local averages of one-dimensional electrical conductivity distributions

Peter Weidelt

Institut für Geophysik und Meteorologie, Technische Universität Braunschweig, D-38106 *Braunschweig, Germany*

Accepted 1995 May 29. Received 1995 May 18; in original form 1995 January 13

SUMMARY

Of particular importance in a non-unique geophysical inverse problem is the unique solution that yields extremal values of a model property of geophysical interest. In the 1-D magnetotelluric inverse problem, we choose the arithmetic average $\bar{\sigma}(z_1, z_2)$ of the electrical conductivity $\sigma(z)$ in a given depth range $z_1 \le z \le z_2$ as such a property, and determine the upper and lower bounds of $\bar{\sigma}(z_1, z_2)$ such that $\sigma(z)$ is compatible with given (noisy) complex impedances for M frequencies. In addition, we impose an *a priori* constraint on $\sigma(z)$ such that $\sigma_- \le \sigma(z) \le \sigma_+$, $0 \le z < \infty$, with pre-assigned bounds σ_- and σ_+.

For a modest number of data, it is possible to derive the exact extremal models. In the one-frequency case ($M = 1$) the extremal models consist of a sequence of uniform layers with conductivities σ_- and σ_+ terminated by an infinite periodic sequence of layers with thicknesses $\pi/2$ times the local penetration depth ($\lambda/4$-plates). For $M > 1$, in addition to uniform layers, transitional layers with a continuous conductivity distribution occasionally occur, and the model structure at great depth asymptotically approaches the periodic structure of the lowest frequency. If *a priori* information is not incorporated ($\sigma_- = 0$, $\sigma_+ = \infty$), the extremal models consist—in the case of exact data—of at least $M + 1$ thin sheets separated by insulators. Therefore the exact extremal models are highly structured. The model structure for selected data sets is displayed in triangular (z_1, z_2)-diagrams, which for $M > 1$ clearly display the complexity of the underlying non-linear problem.

As a by-product of the constrained one-frequency case, we determine the exact range of possible values of apparent conductivities and phases that can be obtained for given values of σ_- and σ_+.

Key words: extremal problem, inverse problem, magnetotellurics.

1 INTRODUCTION

All methods of geophysical inversion, which try to interpret *real* data, are methods of optimization. Whereas traditional approaches search for the model that minimizes the misfit between measured and modelled data, more recent approaches pre-assign the misfit and place emphasis on the construction of the model that extremizes a model property of geophysical interest. Prominent representatives of the latter strategy are the minimum-structure models (e.g. Constable, Parker & Constable 1987; Smith & Booker 1988) and the models leading to maximum-depth rules (e.g. Smith 1959, 1960; Parker 1974, 1975). The actual structure of the extremal models is in general of subordinate interest. What is learnt from the inversion is the extremal value of the model property under investigation, because this number is a bound, which all other competing—and possibly more realistic—models have to satisfy.

This paper considers the simplest problem of magnetotellurics, where the electrical conductivity σ depends on depth z only. For any finite set of data, even if it is accurate, point estimates of the electrical conductivity become meaningless, since at a specified depth level one may introduce either a thin highly conducting sheet or a thin insulating layer without changing the fit to the data. Therefore at a specified depth the conductivity may range between zero and infinity. Of geophysical interest, however, are estimates of the conductivity in a given depth *range* rather than point estimates. If the assigned depth range is sufficiently extended and shallow, the longer periods may be inconsistent with a depth range that is completely filled with material of the highest conductivity, or—on the other hand—the observed damping may be inconsistent with an extended poorly conducting layer. Therefore the average conductivity in the depth range considered can be constrained by the data. The possibility of putting constraints

on linear averages of the conductivity is in accord with the fact that the inverse problem for the conductance (i.e. integrated conductivity) is well-posed (Berdichevskiy & Dmitriev 1992, pp. 198–201).

For a given set of M frequency-dependent surface impedances, we construct those extremal models that maximize or minimize the arithmetic average of σ in the given depth range $z_1 \le z \le z_2$. Moreover, σ may be subjected to the *a priori* constraints $\sigma_- \le \sigma(z) \le \sigma_+$, with σ_- and σ_+ prescribed.

Problems of this kind have been treated previously by Oldenburg (1983) and Dosso & Oldenburg (1989). After discretizing the conductivity structure, the authors reduce the problem of determining the bounds to a problem in nonlinear programming. Starting with an initial guess and linearizing the functional, which maps the conductivity onto the data, the problem is solved iteratively by a sequence of linear programming problems.

The special problem of extremizing the conductivity integrated between the surface $z_1 = 0$ and the level z_2 for the unconstrained case $\sigma_- = 0$, $\sigma_+ = \infty$ has been considered by Weidelt (1985; hereafter W1). W1 explores, in a fully nonlinear treatment, the exact structure of the extremal models for a small number of data. The present paper extends the results of W1 by assuming a depth range $z_1 \le z \le z_2$ and finite *a priori* bounds $\sigma_- \ge 0$ and $\sigma_+ \le \infty$. A simple structure is obtained only in the one-frequency case, where $\sigma(z)$ is found to flip between the extremes σ_- and σ_+. For $M > 1$, additional transitional continuous conductivity variations may occur.

The methods of Oldenburg (1983) and Dosso & Oldenburg (1989) on the one hand and those of W1 and the present paper on the other are complementary: the former approximate approach is robust, computationally efficient, flexible, and suitable for a large data set; the latter exact approach is computationally awkward in the case of many frequencies, but sheds a clearer light on the nature of the underlying problem.

The contents of this paper are as follows. Section 2 gives an outline of the general method for constructing exact extremal models. Section 3 provides a complete survey of the one-frequency case, whereas partial results for the general M-frequency case are presented in Section 4. Applications to synthetic and real data are given both in Sections 3 and 4. The Appendix lists useful results on the electromagnetic induction in a stack of thin sheets (to which the extremal models degenerate in the unconstrained case) and provides detailed information about the structure of the unconstrained one-frequency extremal models.

2 BASIC EQUATIONS AND NECESSARY EXTREMAL CONDITIONS

Attention is confined to a 1-D conductivity profile $\sigma(z)$, z positive downwards, and a uniform inducing magnetic field in the y-direction. Assuming a time factor $e^{i\omega t}$, $\omega > 0$, throughout, the field equations in the quasi-static limit are

$$E_x'(z,\omega) = -i\omega\mu_0 H_y(z,\omega), \qquad H_y'(z,\omega) = -\sigma(z)E_x(z,\omega),$$

where the prime denotes differentiation with respect to z. They lead to the differential equation

$$f''(z,\omega) = i\omega\mu_0\sigma(z)f(z,\omega), \tag{1}$$

with

$$f(z,\omega) := -E_x(z,\omega)/E_x'(0^-,\omega),$$

where the discontinuity of E_x' due to a possible thin conducting surface sheet has been taken into account. The boundary conditions imposed on $f(z)$ are

$$f'(0^-) = -1, \qquad f'(\infty) = 0. \tag{2}$$

In the following, we use Schmucker's response function (Schmucker 1970, p. 69):

$$c(\omega) := \frac{E_x(0,\omega)}{i\omega\mu_0 H_y(0^-,\omega)} = f(0,\omega),$$

with $c = g - ih = |c|\exp(-i\psi)$, $g, h > 0$, which is related to the apparent resistivity ρ_a, impedance Z and impedance phase φ by

$$\rho_a = \omega\mu_0|c|^2, \qquad Z = i\omega\mu_0 c, \qquad \varphi = 90^\circ - \psi.$$

A set of M frequencies ω_j, $j \in [1, M]$ is considered, with the measured responses $c_j := c(\omega_j)$ being either exact or corrupted by noise with the standard deviations s_j. In addition, let $c_j[\sigma] = f(0,\omega_j)$ be the data functional, i.e. the result of solving (1) with the boundary conditions (2) for the conductivity profile $\sigma(z)$ and the frequency ω_j. Hence $\sigma(z)$ is an acceptable model if, in the case of exact data,

$$c_j = c_j[\sigma], \qquad j = 1, \ldots, M, \tag{3}$$

or if, in the case of noisy data, the soft χ^2-bound

$$\sum_{j=1}^{M} |c_j - c_j[\sigma]|^2/s_j^2 \le B \tag{4}$$

is satisfied, where $B := \chi^2_{2M;\alpha}$ is the threshold, which for $2M$ degrees of freedom is exceeded with probability α.

Apart from degenerate data, for example

$$c_j = \frac{a}{b + i\omega_j}, \qquad a > 0,\ b \ge 0,$$

for which in the case of exact data and $M > 1$ only a single conductivity model exists, there will be a whole family of acceptable conductivity profiles. After pre-assigning a depth range $z_1 \le z \le z_2$ and an *a priori* conductivity range

$$\sigma_- \le \sigma(z) \le \sigma_+, \qquad 0 \le z < \infty, \tag{5}$$

we will try to find the model that minimizes or maximizes

$$\bar\sigma(z_1, z_2) := \frac{1}{\Delta}\int_{z_1}^{z_2} \sigma(z)\,dz, \qquad \Delta := z_2 - z_1,$$

subject to the constraints (3) [or (4)] and (5). The extremal averages are $\bar\sigma_{\min}(z_1, z_2)$ and $\bar\sigma_{\max}(z_1, z_2)$. Hence the objective function to be minimized is

$$Q[\sigma] = \int_0^\infty w(z)\sigma(z)\,dz,$$

with the weight function

$$w(z) = \begin{cases} 0, & z \notin (z_1, z_2) \\ +1/\Delta, & z \in (z_1, z_2), \quad Q \to +\bar\sigma_{\min}(z_1, z_2) \\ -1/\Delta, & z \in (z_1, z_2), \quad Q \to -\bar\sigma_{\max}(z_1, z_2). \end{cases} \tag{6}$$

The constraints (3) to (5) are taken into account by Lagrangian multipliers; see for example Avriel (1976) for a concise treatment. In the case of exact data (3) the Lagrange function is

$$L[\sigma] = Q[\sigma] + \mathscr{R}e \sum_{j=1}^{M} \lambda_j \{c_j[\sigma] - c_j\} + \int_0^\infty [\mu_+(z)\{\sigma(z) - \sigma_+\} + \mu_-(z)\{\sigma_- - \sigma(z)\}]\, dz, \quad (7)$$

where $\mathscr{R}e$ denotes the real part. In the case of noisy data (4) the second term on the right-hand side is replaced by

$$\Lambda \left\{ \sum_{j=1}^{M} |c_j[\sigma] - c_j|^2 / s_j^2 - B \right\}. \quad (8)$$

Real and imaginary parts of the complex ordinary Lagrangian multipliers λ_j, which enforce equality constraints, are unrestricted in sign, whereas the generalized Lagrangian multipliers Λ and $\mu_\pm(z)$, which account for inequality constraints, are sign-restricted and non-negative in the present definitions. In particular, these multipliers are zero whenever the constraints are inactive, and non-negative if the constraints are binding. Therefore the expressions (8) and

$$\mu_\pm(z)[\sigma(z) - \sigma_\pm], \qquad 0 \le z < \infty$$

always vanish. The Lagrangian multipliers λ_j and Λ are closely related to the sensitivity of the minimum value Q_0 of $Q[\sigma]$ to changes in the data. Let $c_j =: g_j - ih_j$. Then

$$\mathscr{R}e\, \lambda_j = -\frac{\partial Q_0}{\partial g_j}, \qquad \mathscr{I}m\, \lambda_j = -\frac{\partial Q_0}{\partial h_j}, \qquad \Lambda = -\frac{\partial Q_0}{\partial B}, \quad (9)$$

where $\mathscr{I}m$ denotes the imaginary part. The last equation expresses the obvious fact that an increase in the active χ^2-bound leads to a further decrease in Q_0. The functions $\mu_\pm(z)$ describe the sensitivity of Q_0 to local changes of the conductivity bounds $\sigma_\pm$ at position z. If in a small range δz around z the bounds $\sigma_\pm$ are increased to $\sigma_\pm + \sigma_0$, then with $\delta\tau_\pm(z) := \sigma_0 \delta z$ one obtains in the limit $\delta z \to 0$

$$\mu_\pm(z) = \mp \frac{\partial Q_0}{\partial \tau_\pm(z)}; \quad (10)$$

i.e., if $\sigma(z) = \sigma_-$, implying $\mu_-(z) \ge 0$, an increase of σ_- will not lead to a deeper minimum Q_0, whereas for $\sigma(z) > \sigma_-$, implying $\mu_-(z) = 0$, the change of an inactive bound does not affect Q_0. A similar interpretation holds for $\mu_+(z)$ and σ_+. The sensitivity of Q_0 to a global change of $\sigma_\pm$ is given by

$$\int_0^\infty \mu_\pm(z)\, dz = \mp \frac{\partial Q_0}{\partial \sigma_\pm}.$$

As a necessary extremal condition, the first variation of the Lagrangian $L[\sigma]$ with respect to $\sigma(z)$ has to vanish. Whereas the first and third terms on the right-hand side of (7) are linear in σ and pose no problems, the first variation of the non-linear data functional $c_j[\sigma]$ has to be expressed in terms of its Fréchet derivative $F_j(z)$ defined by

$$\delta c_j[\sigma] = \int_0^\infty F_j(z)\delta\sigma(z)\, dz, \quad (11)$$

with

$$F_j(z) = -i\omega_j \mu_0 f_j^2(z), \quad (12)$$

where $f_j(z) := f(z, \omega_j)$ is the solution of (1) with the boundary conditions (2) (e.g. Parker 1977). Hence $\delta L[\sigma] = 0$ implies, for the exact data case (3),

$$w(z) + \mathscr{R}e \sum_{j=1}^{M} \lambda_j F_j(z) + \mu_+(z) - \mu_-(z) = 0. \quad (13)$$

In the case of noisy data, λ_j in (13) is replaced by

$$\bar{\lambda}_j := 2\Lambda(c_j[\sigma] - c_j)^*/s_j^2, \quad (14)$$

where * denotes the complex conjugate.

In what follows, the necessary condition (13) is used to define the control function

$$D(z) := w(z) + \mathscr{R}e \sum_{j=1}^{M} \lambda_j F_j(z) = \mu_-(z) - \mu_+(z), \quad (15)$$

which states that

$$\begin{aligned} &D(z) \ge 0, \quad \text{when } \sigma(z) = \sigma_-, \\ &D(z) = 0, \quad \text{when } \sigma_- < \sigma(z) < \sigma_+, \\ &D(z) \le 0, \quad \text{when } \sigma(z) = \sigma_+. \end{aligned} \quad (16)$$

It is stressed that—in exceptional situations—only the weak condition $D(z) = 0$, rather than strict positivity or negativity, can be achieved in a depth interval where a conductivity constraint is active; see, for instance, the simple examples given in Section 3.2.3.

The process of model construction therefore consists in selecting a model, within the class of models satisfying the data in the sense of (3) or (4), for which there exists a linear combination $D(z)$ of its Fréchet derivatives that, according to (16), is non-negative (non-positive) where $\sigma(z)$ attains its lower (upper) bound.

The problems with this prescription are at least three-fold.

(1) It does not lead to an immediate model construction, since in general $\sigma(z)$ has to be determined iteratively on the basis of the information on $\sigma(z)$ obtained from the sign changes of $D(z)$.

(2) There might be more than one model satisfying this necessary condition. In order to single out the extremal model, one has to be sure that all these admissible models are known.

(3) The structure of possible extremal models is not known at the outset: does it consist only of discrete layers or do continuous conductivity variations occur in addition? How many layers are required?

Despite these complications, satisfactory model constructions are possible in many cases, since it turns out that in most instances the conductivity only flips between the extremes σ_- and σ_+. This holds in particular for the modest one-frequency case, which is considered in detail in the next section. Moreover, it is often easy to find the pertinent extremal model for small z_1 and z_2. By gradually deforming this solution and monitoring the change of $D(z)$, it is possible to decide for which parameter combination (z_1, z_2) the type of the model has to change, for example where a conducting layer at the surface or at z_1 emerges or disappears, where two conducting layers coalesce, or where a continuous conductivity variation is required in some section of the model. These changes, of course, reflect the full non-linearity, which we take into account.

3 EXTREMAL AVERAGES FOR ONE FREQUENCY

3.1 General structure of the extremal models

If σ_- and σ_+ are suitably chosen such that feasible models exist (Section 3.3.2), the one-frequency extremal models have the property that $\sigma(z)$ only attains the values σ_- and σ_+. Similarly to W1, this is proved by contradiction by assuming that there exists a depth interval (a, b) completely inside or outside (z_1, z_2) such that $\sigma_- < \sigma(z) < \sigma_+$ for $z \in (a, b)$. Then, according to (16), $D(z)$ and all its derivatives vanish identically for $z \in (a, b)$. By dropping the subscript j identifying the frequency for the case $M = 1$, and using the fact that $w(z)$ is piecewise constant, the first and second derivatives of $D(z)$ yield, with reference to (15),

$$\mathscr{R}e[\lambda F'(z)] = 0, \qquad \mathscr{R}e[\lambda F''(z)] = 0.$$

These two homogeneous linear equations for λ have to satisfy the compatibility condition

$$\mathscr{I}m[F''(z)/F'(z)] = 0.$$

However, from (12) and (1) it follows that

$$\begin{aligned}\mathscr{I}m[F''(z)/F'(z)] &= -\mathscr{I}m[i\omega\mu_0\sigma(z)c(z) + 1/c(z)] \\ &= -[\omega\mu_0\sigma(z)g(z) + h(z)/|c(z)|^2] < 0,\end{aligned}$$

since $g(z)$ and $h(z)$ are positive as the real part and negative imaginary part of the response function c at level z:

$$c(z) = -f(z)/f'(z) = g(z) - ih(z).$$

Hence the compatibility condition cannot be satisfied and no continuous conductivity section exists. This conclusion holds for both exact and noisy data.

3.2 Unconstrained conductivity models

3.2.1 General features

In Section 3.2 it is assumed that no constraint (except non-negativity) is imposed on $\sigma(z)$, such that $\sigma_- = 0$, $\sigma_+ = \infty$. According to Section 3.1 the extremal models therefore consist of a stack of K thin sheets of finite conductance τ_k at level ζ_k,

$$\sigma(z) = \sum_{k=1}^{K} \tau_k \delta(z - \zeta_k), \tag{17}$$

terminated possibly be an additional perfectly conducting sheet at ζ_{K+1}. As yet, K is unspecified. A thin sheet is the limit of a conducting layer, for which the conductivity increases to infinity and at the same time the thickness shrinks to zero, such that the conductance, as the product of conductivity and thickness, remains finite.

From (1), (17), and the definition (12), it follows that between adjacent sheets $f(z)$ varies linearly and $F(z)$ quadratically, and across sheets they show a jump in their derivatives. Taking τ and ζ as a generic pair of sheet parameters, the jump relations are

$$f'(\zeta^+) - f'(\zeta^-) = i\omega\mu_0\tau f(\zeta), \tag{18}$$

$$F'(\zeta^+) - F'(\zeta^-) = 2i\omega\mu_0\tau F(\zeta). \tag{19}$$

From $\partial\sigma/\partial\tau = \delta(z - \zeta)$ and $\partial\sigma/\partial\zeta = -\tau\delta'(z - \zeta)$ it follows by using the definition of the Fréchet derivative (11) and the jump relation (18) that

$$\frac{\partial c[\sigma]}{\partial\tau} = F(\zeta) = -i\omega\mu_0 f^2(\zeta), \tag{20}$$

$$\frac{\partial c[\sigma]}{\partial\zeta} = \tau\overline{F'}(\zeta) = [f'(\zeta^-)]^2 - [f'(\zeta^+)]^2, \qquad \tau < \infty, \tag{21}$$

$$\frac{\partial c[\sigma]}{\partial\zeta} = [f'(\zeta^-)]^2, \qquad \tau = \infty. \tag{22}$$

Eq. (21) was obtained after integration by parts using

$$\begin{aligned}-\int_0^\infty F(z)\delta'(z - \zeta)\,dz &= \int_0^\infty F'(z)\delta(z - \zeta)\,dz \\ &= [F'(\zeta^-) + F'(\zeta^+)]/2 \\ &=: \overline{F'}(\zeta).\end{aligned}$$

The depth levels that are distinguished are z_1, z_2 and $z = 0$, the latter as the plane of observation and natural boundary of the conductor. Sheets at these positions cannot move freely and are defined by their conductance only. On the other hand, a mobile sheet has its position as the second free parameter. An exception is the possibly existing final sheet of infinite conductance, which again is defined by only one parameter.

The following three properties of one-frequency extremal models are easily derived.

(1) No mobile sheet of finite conductance τ can exist at $\zeta \notin (z_1, z_2)$. A final mobile sheet of *infinite* conductance, however, may occur.

(2) The extremal model for $\bar{\sigma}_{\max}$ cannot have a mobile sheet at $\zeta \in (z_1, z_2)$, whereas at most one mobile sheet appears in the models for $\bar{\sigma}_{\min}$.

(3) The extremal models for $\bar{\sigma}_{\max}$ terminate with a mobile sheet of infinite conductance at $z = \zeta_\infty$ below a sheet at $z = z_2^-$, whereas the extremal models for $\bar{\sigma}_{\min}$ end with an insulator below a sheet at $z = z_2^+$.

Before presenting the proofs, the necessary extremal conditions outlined in Section 2 have to be briefly reviewed for the present unconstrained conductivities. Since only a lower bound (non-negativity) is imposed on $\sigma(z)$, the Lagrangian multiplier function $\mu_+(z)$ vanishes identically and the control function $D(z)$, defined in (15), is non-negative. In particular it has to vanish at a position ζ of a thin sheet, since the non-negativity constraint is not active there. If the sheet is mobile, the average slope of $D(z)$ vanishes at ζ, thus avoiding negative values ('double-zero'). Therefore necessary conditions for a mobile sheet of finite τ are

$$D(\zeta) = w(\zeta) + \mathscr{R}e[\lambda F(\zeta)] = 0, \qquad \overline{D'}(\zeta) = \mathscr{R}e[\lambda\overline{F'}(\zeta)] = 0, \tag{23}$$

expressing just the insensitivity of the minimum Q_0 to small changes of τ and ζ. A perturbation $\delta\tau$, for instance, affects Q_0 in two ways: it perturbs Q_0 by $\delta Q_0^{(1)} = w(\zeta)\delta\tau$, and it perturbs c according to (20) for $\delta c = F(\zeta)\delta\tau$. Since the response c has to remain unchanged, we have to calculate the modification $\delta Q_0^{(2)}$ resulting from the response $c - \delta c$. The first two equations of (9) immediately yield $\delta Q_0^{(2)} = -\mathscr{R}e[\lambda(-\delta c)] = \mathscr{R}e[\lambda F(\zeta)]\delta\tau$, such that according to (23) $\delta Q_0^{(1)} + \delta Q_0^{(2)} = 0$.

Proof of Proposition 1

One has simply to note that $w(\zeta)=0$ for $\zeta \notin (z_1, z_2)$, such that the existence of a solution depends on the compatibility condition $\mathscr{Im}[\overline{F'}(\zeta)/F(\zeta)]=0$. From (21), (20) and (18) it follows, however, that

$$\overline{F'}(\zeta)/F(\zeta)=[f'(\zeta^+)+f'(\zeta^-)]/f(\zeta)=-(1/c^+ + 1/c^-),$$

where c^+ and c^- are the responses below and above the sheet, which both have a negative imaginary part. Therefore the compatibility condition cannot be satisfied.

A final sheet with $\tau=\infty$ at ζ can exist, since in view of the fact that $F(\zeta)=0$ the first equation of (23) is satisfied automatically. For the second equation, (22) has to be used. If the sheet adjacent to ζ is at $z=\eta<\zeta$, then

$$f'(\zeta^-)=f'(\eta^+)=-f(\eta)/(\zeta-\eta),$$

such that with reference to (12) and (22) the second equation of (23) is cast into the convenient form

$$\mathscr{Im}[\lambda F(\eta)]=0, \tag{24}$$

which we will use in the next section.

Proof of Proposition 2

We first show that $\bar{\sigma}_{\max}$ has no mobile sheet at $\zeta \in (z_1, z_2)$. Assuming a sheet at $z=z_2^-$ (*cf.* Proposition 3) the conditions to be satisfied are

$$\mathscr{Re}[\lambda F(\zeta)]=1/\Delta,$$

$$\mathscr{Re}[\lambda \overline{F'}(\zeta)]=0,$$

$$\mathscr{Re}[\lambda F(z_2)]=1/\Delta.$$

These three linear equations for the complex multiplier λ require the compatibility condition

$$\mathscr{Im}[\overline{F'}(\zeta)/\{F(z_2)-F(\zeta)\}]=0.$$

From (A7) it follows that

$$f(z_2)=f(\zeta)(1-d/c^+),$$

with $d:=z_2-\zeta$. Therefore

$$\frac{\overline{F'}(\zeta)}{F(z_2)-F(\zeta)}=\frac{1/c^- + 1/c^+}{2d/c^+ - (d/c^+)^2}=\frac{2+i\omega\mu_0\tau c^+}{d(2-d/c^+)}, \tag{25}$$

where according to (A5) $1/c^- = 1/c^+ + i\omega\mu_0\tau$. Eq. (A6) yields $c^+ = c(z_2^-)+d$. Since $\mathscr{Re}\, c(z_2^-)\geq 0$, we have $\mathscr{Re}\, c^+ \geq d$, which implies $\mathscr{Re}(d/c^+)\leq 1$. Moreover, $\mathscr{Im}(d/c^+)>0$. Therefore the real parts of the numerator and denominator in the last fraction of (25) are of the same sign, and the imaginary parts are of opposite sign. Hence the compatibility condition cannot be satisfied.

A mobile sheet at $\zeta \in (z_1, z_2)$ can exist, however, in the extremal models for $\bar{\sigma}_{\min}$. Assuming a sheet at z_2^+, the compatibility condition $\mathscr{Im}[\overline{F'}(\zeta)/F(z_2)]=0$ resulting from the system

$$\mathscr{Re}[\lambda F(\zeta)]=-1/\Delta,$$

$$\mathscr{Re}[\lambda \overline{F'}(\zeta)]=0,$$

$$\mathscr{Re}[\lambda F(z_2)]=0$$

can be satisfied. Examples are given in Section 3.2.3. However, a second mobile sheet at $z=\zeta'$ cannot arise. Without restricting generality, let $\zeta'>\zeta$. The relevant equations are then

$$\mathscr{Re}[\lambda F(\zeta)]=-1/\Delta,$$

$$\mathscr{Re}[\lambda \overline{F'}(\zeta)]=0,$$

$$\mathscr{Re}[\lambda F(\zeta')]=-1/\Delta,$$

$$\mathscr{Re}[\lambda \overline{F'}(\zeta')]=0,$$

$$\mathscr{Re}[\lambda F(z_2)]=0.$$

The subsystem consisting of the first three equations has no solution, since it agrees with the incompatible system for $\bar{\sigma}_{\max}$ (with ζ' and $-1/\Delta$ replaced by z_2 and $+1/\Delta$, respectively).

Proof of Proposition 3

This proposition is proved first for $\bar{\sigma}_{\max}$. Assume at the outset that the terminating perfectly conducting sheet is missing, and that the deepest finite-conductance sheet lies at $z=\zeta$. According to Proposition 1 we have $\zeta \leq z_2$. Since $F(z)=$ *constant* for $z>\zeta$, the necessary condition $D(\zeta)=0$ for $\zeta<z_2$ or $D(z_2^-)=0$ for $\zeta=z_2$ leads to $D(z_2^+)=1/\Delta$. As a consequence, $\bar{\sigma}_{\max}$ would be highly and uniformly sensitive to conductivity changes when $z>z_2$, a behaviour which can be excluded. Therefore a perfectly conducting sheet at $z=\zeta_\infty$ has to be assumed, and $D(z)$ in $z_2<z<\zeta_\infty$ is given by $D(z)=A(\zeta_\infty - z)^2$ with $D(z_2)\geq 1/\Delta$. If the sheet at $z=z_2^-$ were absent, $D(z)$ would simply decrease by $1/\Delta$ when passing $z=z_2$ from below, but would continue to increase when moving upwards such that it would be impossible to satisfy $D(\zeta)=0$ at the first conducting sheet encountered at $z=\zeta$. A sheet at z_2^-, however, changes the slope and curvature of $D(z)$ and fulfils the condition $D(\zeta')=0$ with $\zeta'=z_1$ or $\zeta'=0$. The sheet at z_2^- still contributes to $\bar{\sigma}_{\max}(z_1, z_2)$.

If, on the other hand, $\bar{\sigma}_{\min}$ were to terminate with a perfectly conducting sheet at $z=\zeta_\infty$, then $D(z)=A(\zeta_\infty - z)^2$, $A\geq 0$ for $z\in(z_2, \zeta_\infty)$. Let ζ be the position of the deepest finite-conductance sheet. If $\zeta<z_2^+$ (i.e. if the sheet at $z=z_2^+$ is absent), then $D(\zeta)=A(\zeta_\infty-\zeta)^2+1/\Delta>0$ and the necessary condition $D(\zeta)=0$ cannot be satisfied. If $\zeta=z_2^+$, then $\mathscr{Re}[\lambda F(z_2)]=0$ (implying $A=0$) and according to (24) $\mathscr{Im}[\lambda F(z_2)]=0$ also. Hence, $\lambda=0$, $D(z)=w(z)$, and $\bar{\sigma}_{\min}$ would be independent of the data, which only holds in exceptional cases (see, for example, the model for Region B in Section 3.2.3). Therefore the models of $\bar{\sigma}_{\min}$ terminate with an insulator, implying $D(z)=0$ for $z>z_2$. If the sheet at $z=z_2^+$ is absent, $D(z)$ would merely increase by $1/\Delta$ when passing $z=z_2$ from below, and the condition $D(\zeta)=0$ could again not be satisfied. The remedy is a conducting sheet at $z=z_2^+$. It does not contribute to $\bar{\sigma}_{\min}(z_1, z_2)$.

3.2.2 *The extremal models for* $\bar{\sigma}_{\max}$

To start with, we assume exact data such that $c=c[\sigma]$. A secure point of departure and arrival is the representation of c by a two-parameter model with a surface sheet of conductance $\tau(0)$ and a perfectly conducting sheet at ζ_∞:

$$c=c[\sigma]=\frac{\zeta_\infty}{1+i\omega\mu_0\tau(0)\zeta_\infty}, \tag{26}$$

with

$$\tau(0)=\frac{h}{\omega\mu_0|c|^2}, \qquad \zeta_\infty=\frac{|c|^2}{g}.$$

It was shown in W1 and by Yee & Paulson (1988) that this model has two extremal properties, namely the *greatest* surface conductance and the *shallowest* perfect conductor of all models fitting c. Hence it is the starting point when z_2 is small. On the other hand, $\bar{\sigma}_{\max}$ will become infinite when $z_2 > \zeta_\infty =: z_{2M}$, whereas it remains finite for $z_1 < z_2 < \zeta_\infty$.

In what follows, the structure of the extremal models and the corresponding extremal averages are displayed for all possible combinations $z_1 < z_2$ in triangular diagrams, for which Fig. 1 is the first example. The data are representative of the c-response of the diurnal Sq-harmonic. The diagram, being bounded by the lines $z_1 = z_2$ and $z_2 = z_{2M}$, shows that four different models are required, the two-parameter model (26) being realized at the top and the base of the triangle.

It was noted in the previous section that for a single frequency, no mobile finite-conductance sheets occur. Therefore possible positions of sheets are only $z = 0, z_1, z_2$, and the unspecified position ζ_∞ of the final perfectly conducting sheet. Region A is essentially the model (26) with the original surface sheet now at $z = z_2$. Region B requires an additional sheet at z_1, and the transitional small region C also requires a surface sheet. In region D the surface sheet subsists, whereas the sheet at z_1 is disappearing. The quadruple point Q is remarkable: the simple model A is realized there, but, by an infinitesimal change of z_1 and/or z_2, the regions B to D with their more complicated models are reached.

The control function $D(z)$, which plays a key role in the model construction, is displayed in Fig. 2 for four pairs (z_1, z_2) from each of the regions. Before entering into a detailed description of the model-finding process, a discussion of this figure might be useful. Since $\sigma_+ = \infty$, the extremal conductivity average $Q_0 = -\bar{\sigma}_{\max}(z_1, z_2)$ is insensitive to small changes of the upper conductivity bound, i.e. according to (10) and (15) $\mu_+(z) \equiv 0$ and $D(z) = \mu_-(z)$. If, in the small range from $z - \delta z/2$ to $z + \delta z/2$, the lower bound σ_- is perturbed from 0 to σ_0, and if $\delta\tau_-(z) := \sigma_0 \delta z$, then in the limit $\delta z \to 0$ (10) yields

$$D(z) = -\frac{\partial \bar{\sigma}_{\max}(z_1, z_2)}{\partial \tau_-(z)}. \tag{27}$$

Consider first a (positive) perturbation $\delta\tau_-(z)$ at $z \in (z_2, \zeta_\infty)$ where the lower bound is active, $\sigma(z) = 0$. To restore the fit to the data, this perturbation has to be compensated by a (smaller) decrease in the conductance $\tau(z_2)$ at the shallower level z_2. Therefore, according to (27), $0 < \Delta D(z) < 1$. If $z \to z_2^+$, the perturbation $\delta\tau_-(z_2^+)$ is simply balanced by decreasing the adjacent conductance $\tau(z_2)$ by $\delta\tau_-(z_2^+)$, and thus decreasing $\bar{\sigma}_{\max}(z_1, z_2)$ by $\delta\tau(z_2^+)/\Delta$. Therefore, according to (27), $\Delta D(z_2^+) = 1$. On the other hand, a perturbation of the lower bound at z_2^- by $\delta\tau_-(z_2^-)$ is again compensated by a corresponding decrease of $\tau(z_2)$, but now the total conductance in the range $[z_1, z_2]$ remains unchanged and therefore $D(z_2^-) = 0$. The conductance increase due to a perturbation $\delta\tau_-(z)$ at a point $z \in (z_1, z_2)$ is also compensated by a decrease in $\tau(z_2)$. Since $z_2 > z$, the skin effect requires that the decrease at z_2 is stronger than the increase at z, leaving a net *decrease* of $\bar{\sigma}_{\max}(z_1, z_2)$, i.e. $D(z) > 0$. If the sheet at z_1 is present, the discussion

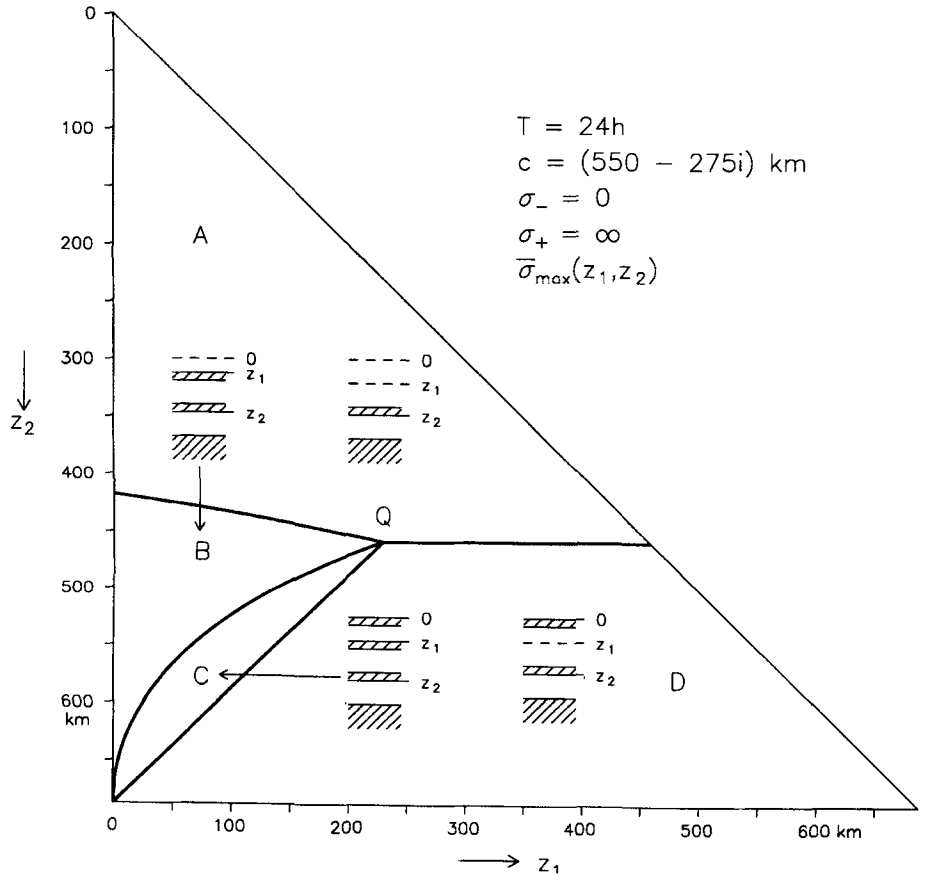

Figure 1. Structure of the unconstrained extremal models for $\bar{\sigma}_{\max}(z_1, z_2)$. The icons representing the position of the conducting sheets are not drawn to scale. All models terminate with a sheet of infinite conductance. Q is the quadruple point, existing only for $g \geq h$.

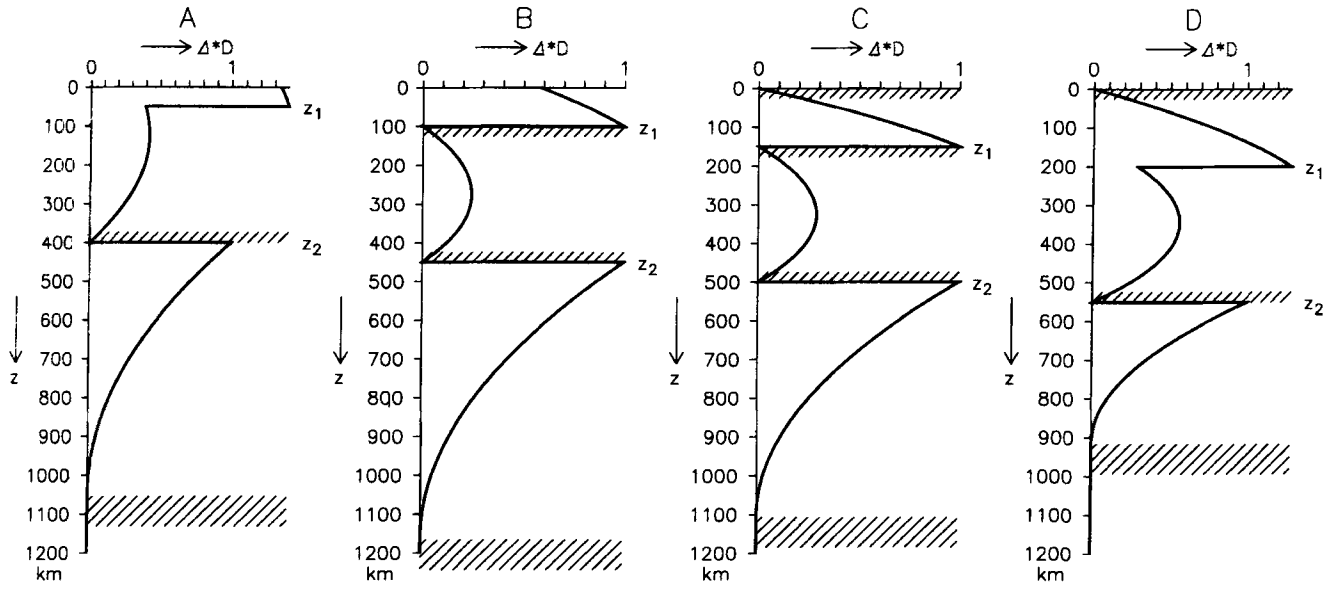

Figure 2. Typical graphs of the control function $D(z)$ for the regions A–D of Fig. 1. In all cases $\Delta = 350$km.

concerning $D(z)$ near $z = z_2$ also pertains to $z = z_1$. If the sheet at z_1 is absent (regions A and D), the perturbations near $z = z_1$ are balanced by a stronger decrease of $\tau(z_2)$. For $z \to z_1^+$, the positive perturbation $\delta\tau_-(z_1^+)$ contributes to $\bar{\sigma}_{\max}(z_1, z_2)$ and partially counteracts the decrease of $\tau(z_2)$, whereas for $z \to z_1^-$ the perturbation is not taken into account in $\bar{\sigma}_{\max}(z_1, z_2)$, such that—at least for region A—its change reflects the full decrease of $\tau(z_2)$.

Region A

The requirements for an extremal model are that the two-sheet model with the two unknown parameters $\tau(z_2)$ and ζ_∞ fits the data and that the objective function $Q[\sigma]$ is insensitive to changes in the model parameters. Therefore, according to (3), (23), and (24) the relevant equations are

$$c[\sigma] = c,$$

$$\mathcal{R}e[\lambda F(z_2)] = 1/\Delta,$$

$$\mathcal{I}m[\lambda F(z_2)] = 0,$$

i.e. four real equations for the two model parameters and the complex λ. The former are easily obtained from the first equation, whereas the two remaining equations serve to determine λ:

$$\lambda = \frac{1}{F(z_2)\Delta}. \tag{28}$$

Since the sheet at z_2 and the final conductor are present in all models, (28) invariably holds for all four regions; the value of $F(z_2)$, however, changes. Using (12) and $f(z) = c - z$, $0 \le z \le z_2$ in region A, we obtain

$$\lambda = -\frac{1}{i\omega\mu_0(c - z_2)^2\Delta}. \tag{29}$$

With the known model parameters and λ, the control function $D(z)$ is easily determined. An example is shown in Fig. 2(A). As a necessary extremal condition, $D(z)$ is non-negative. The discontinuities at z_1 and z_2 are due to $w(z) = -1/\Delta$ for $z \in (z_1, z_2)$, and $w(z) = 0$ elsewhere. Between sheets, $D(z)$ varies quadratically. Model A ceases to be valid as soon as a further increase of z_2 leads to the vanishing of the function $D(z)$ at $z = 0$ or $z = z_1$, signalling the need to introduce an additional sheet. Assuming that first $D(z_1) = 0$ (see Fig. 2B), we enter region B.

Region B

We now need a three-sheet model, where the parameters $\tau(z_1)$, $\tau(z_2)$ and ζ_∞ satisfy

$$c[\sigma] = c,$$

$$\mathcal{R}e[\lambda F(z_1)] = 1/\Delta,$$

$$\mathcal{R}e[\lambda F(z_2)] = 1/\Delta,$$

$$\mathcal{I}m[\lambda F(z_2)] = 0.$$

The last three equations, considered as a linear system for λ, require the compatibility condition

$$\mathcal{R}e[F(z_1)/F(z_2)] = 1, \tag{30}$$

which along with the first (complex) equation determines the three model parameters. λ is then given by (28). Since $\tau(z_1)$ vanishes at the boundary between regions A and B, $f(z) = c - z$, $0 \le z \le z_2$, still applies. Therefore the boundary A–B is defined by

$$\mathcal{R}e\left(\frac{c - z_1}{c - z_2}\right)^2 = 1. \tag{31}$$

After discarding the solution $z_1 = z_2$, this is an algebraic equation of first order in z_1 and third order in z_2, which is easily solved (see Appendix B.1).

Region D

If in model A, $D(z)$ first vanishes at $z = 0$ when z_2 is increased, we pass from region A to region D (see Fig. 2D). The relevant

equations are

$$c[\sigma] = c,$$

$$\mathscr{R}e[\lambda F(0)] = 0,$$

$$\mathscr{R}e[\lambda F(z_2)] = 1/\Delta,$$

$$\mathscr{I}m[\lambda F(z_2)] = 0.$$

The two homogeneous equations in λ are compatible only if

$$\mathscr{R}e[F(z_2)/F(0)] = 0 \quad \text{or} \quad \arg[f(z_2)/f(0)] = -\pi/4, \tag{32}$$

where we have discarded $+\pi/4$ because the phase only decreases with depth. Eq. (32) implies that in extremal models requiring a surface sheet, the electric field at z_2 lags 45° behind its surface value. Eq. (32) and $c[\sigma] = c$ enable the computation of the model parameters $\tau(0)$, $\tau(z_2)$ and ζ_∞.

At the boundary A–D, where $\tau(0)$ still vanishes, (32) reduces to

$$\arg(1 - z_2/c) = -\pi/4 \quad \text{or} \quad z_2 = |c|^2/(g+h). \tag{33}$$

Since no sheet at z_1 is present, the boundary A–D does not depend on z_1.

The quadruple point Q lies at the intersection of the boundaries A–B and A–D. After introducing (33), eq. (31) reduces to $\mathscr{I}m(1 - z_1/c)^2 = -2h^2/(g+h)^2$, such that

$$z_1 = z_{1Q} := \frac{h|c|^2}{g(g+h)}, \qquad z_2 = z_{2Q} := \frac{|c|^2}{g+h}.$$

Since $z_1 \le z_2$, a quadruple point exists only for $h \le g$, i.e. for an impedance phase $\varphi \ge 45°$. If $g < h$, for any z_1 the pertinent models change continuously from A to D when increasing z_2 from 0 to z_{2M}.

Region C

The small intermediate region C has the most complicated structure, since here the sheets at $z = 0$ and $z = z_1$ coexist (Fig. 2C). We have to solve the system of equations

$$c[\sigma] = c,$$

$$\mathscr{R}e[\lambda F(0)] = 0,$$

$$\mathscr{R}e[\lambda F(z_1)] = 1/\Delta,$$

$$\mathscr{R}e[\lambda F(z_2)] = 1/\Delta,$$

$$\mathscr{I}m[\lambda F(z_2)] = 0,$$

where the last four linear equations in λ now require the simultaneous validity of (30) and (32), which in turn, along with $c[\sigma] = c$, are used to determine the four model parameters.

At the boundary C–D, the sheet at z_1 is still absent. Therefore $f(z) = c(1 - z/c^+)$ in $0 \le z \le z_2$, where c^+ with $1/c^+ = 1/c - i\omega\mu_0\tau(0)$ is the response function at $z = 0^+$ below the surface sheet. Hence, the compatibility conditions at the boundary are

$$\arg(1 - z_2/c^+) = -\pi/4,$$

$$\mathscr{R}e[(1 - z_1/c^+)^2/(1 - z_2/c^+)^2] = 1.$$

Solving the first condition for $\tau(0)$, namely $\omega\mu_0\tau(0) = 1/z_{2Q} - 1/z_2$, and inserting the result in the latter, it is found that the boundary C–D is defined by the simple relation

$$z_1 + z_2 = |c|^2/g = z_{2M}.$$

The same principle is followed for the determination of the boundary B–C, where the surface sheet is still missing. We have $f(0) = c$ and $f(z_1) = c - z_1$, whereas $f(z_2)$ has to be expressed in terms of the unknown conductance $\tau(z_1)$. This is determined from (32) and then by inserting $f(z_2)$ into (30), which finally determines the boundary. The explicit expression is given in Appendix B.1.

For the one-frequency data set of Fig. 1, isolines of $\bar{\sigma}_{\max}$ are shown in Fig. 3 in a triangular presentation. As expected, $\sigma_{\max}$ tends to infinity both for $z_1 \to z_2$ and for $z_2 \to z_{2M}$. In the first limit, any thin sheet at z_2 yields an unbounded average conductivity; in the second limit, z_2 approaches the shallowest perfect conductor compatible with the data. Of interest are those parts of the diagram where $\bar{\sigma}_{\max}$ is small, because these averages are constrained by the data. In the present example, the average conductivity between the surface and 275 km is the most constrained: whatever 1-D model we take to fit this two-data set, none will have an average conductivity exceeding 72 mS m^{-1} between 0 and 275 km.

So far, only exact data have been considered. If errors are taken into account, according to (4) we have to satisfy

$$|c[\sigma] - c| \le s, \tag{34}$$

where for simplicity the numerical χ^2-bound is absorbed into s. At the new extremum, (34) is assumed to be satisfied as an equality, i.e. $\Lambda > 0$, since in the case of an inactive constraint, $\Lambda = 0$, the extremum would not depend on the χ^2-bound. Hence the extremal model satisfies

$$c[\sigma] = c + \delta c, \qquad |\delta c| = s.$$

Because of the simplicity of the one-frequency case, one can easily spot the new extremum through a line search on the periphery of the circle $|\delta c| = s$.

If $s/|c|$ is small, however, an approximate first-order determination of the new extremum using the Lagrangian multiplier λ is adequate. Recalling that $Q_0 = -\bar{\sigma}_{\max}$ and $c = g - ih$, eq. (9) yields

$$\delta\bar{\sigma}_{\max} \simeq \mathscr{R}e(\lambda\delta c),$$

which is maximized and minimized for $\arg\delta c = -\arg\lambda$ and $\arg\delta c = \pi - \arg\lambda$, respectively. If $\bar{\sigma}_{\max}$ is the extremum for exact data, the extremum for inexact data will therefore vary between approximately $\bar{\sigma}_{\max} - |\lambda|s$ and $\bar{\sigma}_{\max} + |\lambda|s$, where in the present context only the upper bound of $\bar{\sigma}_{\max}$ is relevant. Taking as an example $\bar{\sigma}_{\max}$ for region A, we have

$$\bar{\sigma}_{\max} = \frac{h}{\omega\mu_0\Delta|c - z_2|^2}.$$

Therefore, using λ from (29),

$$\frac{h - s}{|c - z_2|^2} \le \omega\mu_0\Delta\bar{\sigma}_{\max} \le \frac{h + s}{|c - z_2|^2}. \tag{35}$$

The exact determination by a line search—assuming that s is so small that all points of the periphery lie in region A—provides the slightly asymmetric bounds

$$\frac{h - s}{|c - z_2|^2 - s^2} \le \omega\mu_0\Delta\bar{\sigma}_{\max} \le \frac{h + s}{|c - z_2|^2 - s^2}, \tag{36}$$

which to first order in $s/|c - z_2|$ agree with (35). It is noted, however, that in region A (35) underestimates the relevant upper bound. Even (36) underestimates this bound if the peripheral maximum point lies outside region A. The appropriate

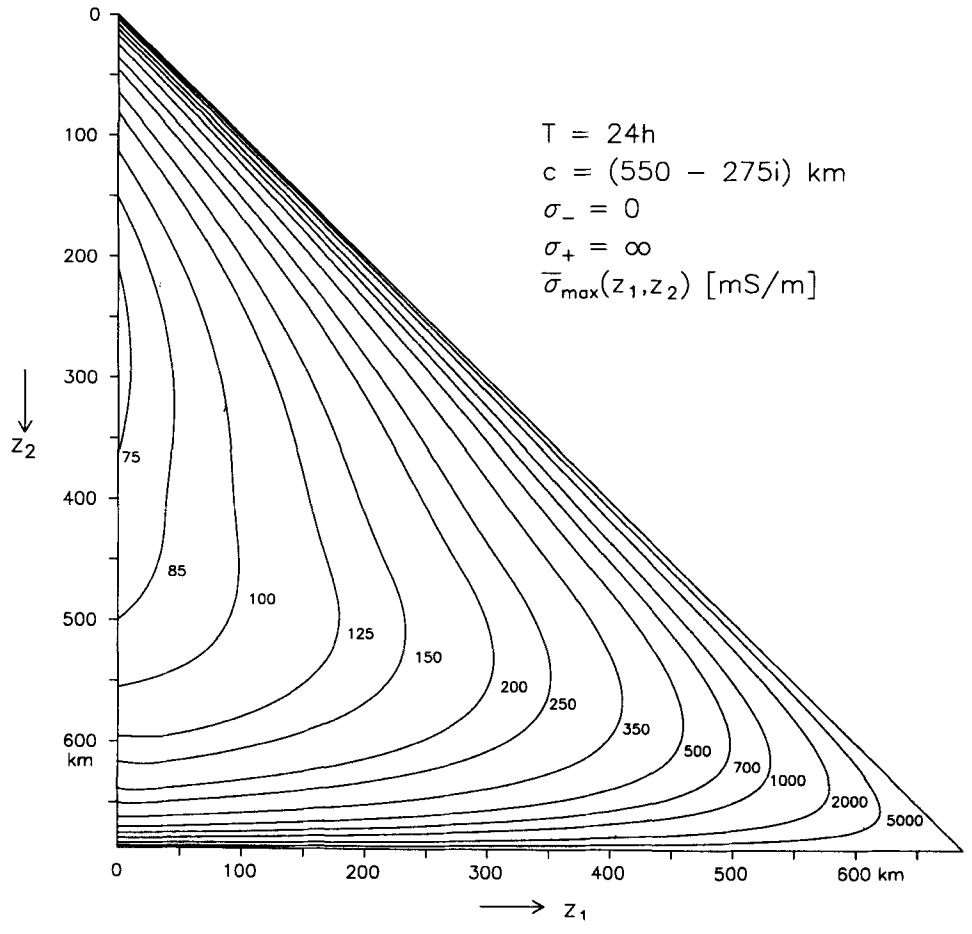

Figure 3. Isolines of $\bar{\sigma}_{max}(z_1, z_2)$ for unconstrained conductivity variations.

method for noisy data in the multifrequency case is described in Section 4.1.4.

Explicit expressions for all parameters of the extremal models in regions A–D and further relevant material is collected in Appendix B.1.

3.2.3 *The extremal models for* $\bar{\sigma}_{min}$

Now the conducting material has to be distributed in such a way that the data are satisfied and the average conductivity between z_1 and z_2 is as small as possible. A major difference to the minimization of the conductance between the surface level and z_2, as considered in W1, is the fact that a possible surface sheet has to be included in the conductance, but is excluded from $\bar{\sigma}_{min}$, since one may consider $z_1 = 0^+$. Therefore the minimal conductance model is not a point of departure for $z_1 \to 0$. Generally, whenever a sheet is required in a $\bar{\sigma}_{min}$-model at the end points of the range of integration, it lies at z_1^- or z_2^+ and does not contribute to $\bar{\sigma}_{min}$.

Therefore in the simple one-frequency problem, for a wide range of parameters (z_1, z_2), conductor configurations exist which yield $\bar{\sigma}_{min}(z_1, z_2) = 0$. Fig. 4 shows the possible situations for $\bar{\sigma}_{min}$. Again, four regions are required to cover the full (z_1, z_2)-space. Here, A and B lead to a vanishing conductivity average, whereas C and D show the anticipated mobile sheet of conductance τ at $\zeta \in (z_1, z_2)$. Representative graphs of $D(z)$ are displayed in Fig. 5. A physical interpretation of $D(z)$ as the sensitivity of $\bar{\sigma}_{min}$ to a perturbation of the lower bound σ_- at depth z,

$$D(z) = \frac{\partial \bar{\sigma}_{min}(z_1, z_2)}{\partial \tau_-(z)}$$

[*cf.* also (27)], is again rewarding. For instance, the perturbation of the data due to a positive perturbation of this bound near $z = \zeta$ can be compensated by a corresponding decrease of τ, such that $\bar{\sigma}_{min}(z_1, z_2)$ remains unchanged, and therefore $D(\zeta) = 0$. On the other hand, a positive perturbation at $z \in (\zeta, z_2)$ is balanced by a reduction of both τ *and* $\tau(z_2)$, and therefore leads to a net increase of $\bar{\sigma}_{min}(z_1, z_2)$, since the sheet at z_2^+ does not contribute to $\bar{\sigma}_{min}$. Perturbations in $z > z_2$ are fully compensated by $\tau(z_2)$ and hence do not affect $\bar{\sigma}_{min}$.

Region A

The data c can be interpreted by a two-parameter model consisting of a single sheet of conductance τ at depth ζ:

$$c = g - ih = \zeta + \frac{1}{i\omega\mu_0\tau}. \tag{37}$$

Therefore $\bar{\sigma}_{min}(z_1, z_2) = 0$ whenever (z_1, z_2) lies below this sheet, $g < z_1 < z_2$. In this region, $\bar{\sigma}_{min}$ does not depend on infinitesimal changes of the data. Hence, $\lambda = 0$ and $D(z) = w(z)$. Since $w(z) \geq 0$ according to (6), the extremal condition (16) is satisfied with

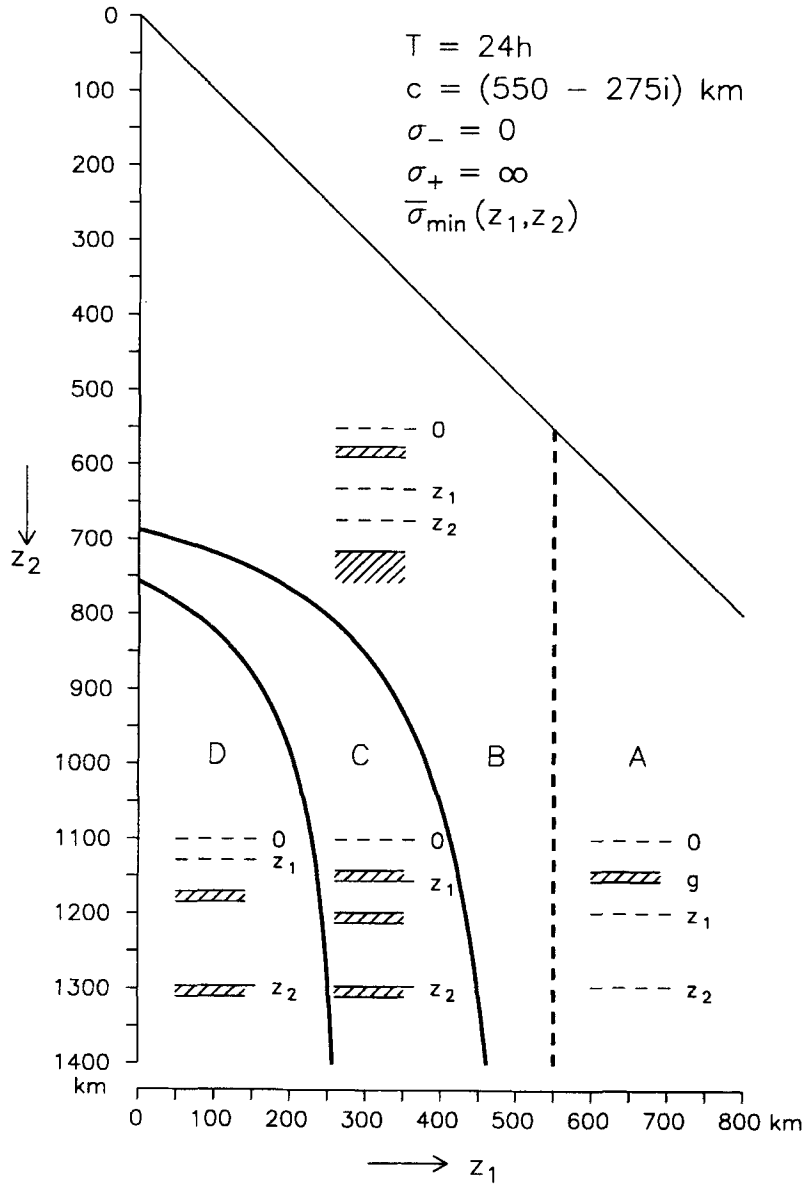

Figure 4. Structure of the unconstrained extremal models for $\bar{\sigma}_{\min}(z_1, z_2)$. For $z_2 \to \infty$ the boundary B–C approaches the dashed line $z_1 = g$. Region D exists only for $g \geq h$. The models giving $\bar{\sigma}_{\min}(z_1, z_2) = 0$ are non-unique.

$D(z) = 0$ for $z \notin (z_1, z_2)$. This is a trivial example where equality holds in (16) although $\sigma(z)$ attains its lower bound.

Region B

The data c can also be interpreted by a three-parameter model consisting of a thin sheet of conductance τ at $z = \zeta < g$ and a perfectly conducting sheet at ζ_∞:

$$\frac{1}{c-\zeta} = i\omega\mu_0\tau + \frac{1}{\zeta_\infty - \zeta},$$

where, taking the real part, ζ and ζ_∞ are related by $\zeta_\infty = g + h^2/(g-\zeta)$. Therefore $\bar{\sigma}_{\min}(z_1, z_2) = 0$ also if $(z_1, z_2) \in (\zeta, \zeta_\infty)$. Here again $D(z) = w(z)$.

In regions A and B the conductivity $\sigma(z)$ is not completely specified for $z \notin (z_1, z_2)$, except for the modest requirement that it should fit the data. However, the extremal models become unique and $\bar{\sigma}_{\min} > 0$, when (z_1, z_2) can no longer be accommodated in (ζ, ζ_∞). Therefore the boundary between regions B and C in Fig. 4 is defined by $z_1 = \zeta$, $z_2 = \zeta_\infty$, i.e.

$$z_2 = g + \frac{h^2}{g - z_1} = z_1 + \frac{|c - z_1|^2}{g - z_1}. \tag{38}$$

Region C

Now a mobile sheet of conductance τ at $z = \zeta \in (z_1, z_2)$ is required. The relevant system of equations is

$$c[\sigma] = c, \tag{39}$$

$$\mathcal{R}e[\lambda F(z_1)] = 0, \tag{40}$$

$$\mathcal{R}e[\lambda F(\zeta)] = -1/\Delta, \tag{41}$$

$$\mathcal{R}e[\lambda \overline{F'}(\zeta)] = 0, \tag{42}$$

$$\mathcal{R}e[\lambda F(z_2)] = 0, \tag{43}$$

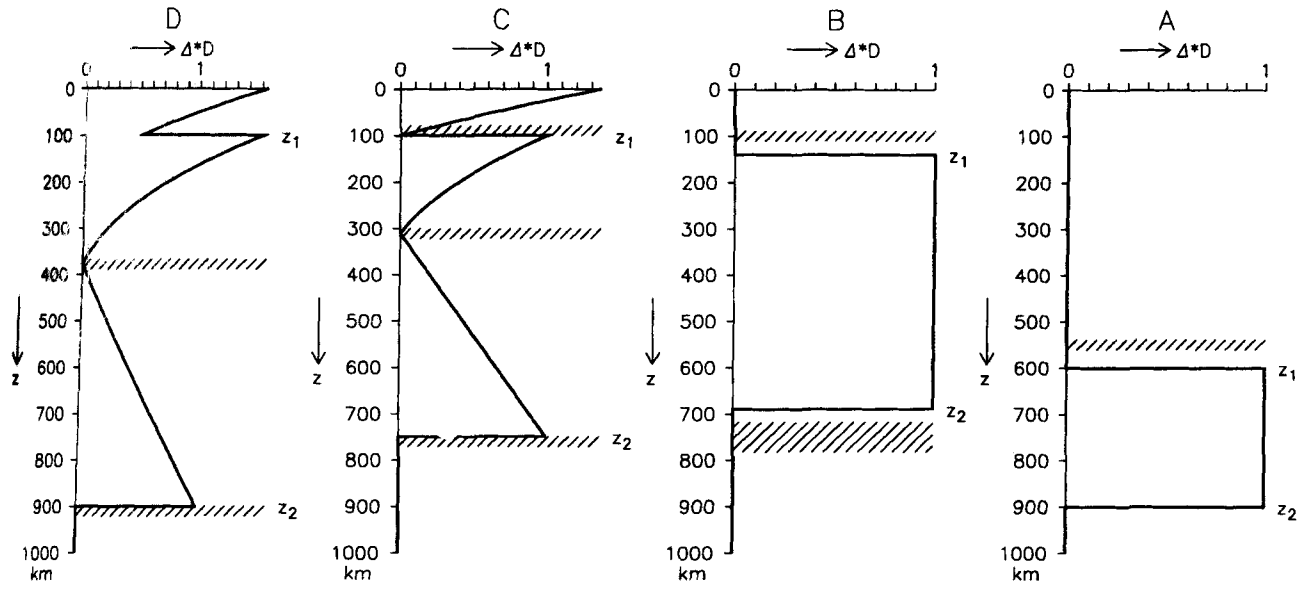

Figure 5. Typical graphs of $D(z)$ for the regions A–D of Fig. 4. In panels A and B we have $D(z) = w(z)$, i.e. the extremum is insensitive to small changes in the data.

which accounts for the fact that the sheets actually lie at z_1^- and z_2^+, where $w(z) = 0$. The homogeneous equations require the two compatibility conditions

$$\mathcal{I}m[\overline{F}'(\zeta)/F(z_1)] = 0, \qquad \mathcal{I}m[\overline{F}'(\zeta)/F(z_2)] = 0, \tag{44}$$

which, along with (39), form a system of four non-linear equations for the model parameters $\tau(z_1)$, τ, ζ, and $\tau(z_2)$. The closed-form solution is given in Appendix B.2. The Lagrangian multiplier is

$$\lambda = \frac{i}{F(z_2)\,\mathcal{I}m[F(\zeta)/F(z_2)]\Delta}. \tag{45}$$

Whereas the model parameters change more or less continuously at the boundary B–C, $D(z)$ undergoes a discontinuous change, as is evident from a comparison of panels B and C of Fig. 5. We shall briefly study this peculiar behaviour. Let

$$y := (g - z_1)\Delta/|c - z_1|^2.$$

Then the boundary B–C, eq. (38), is given by $y = 1$ with $y > 1$ in region C. Let $y = 1 + \varepsilon$ with $0 < \varepsilon \ll 1$. From the results in Appendix B.2 it follows, retaining only the leading order in ε, that

$$\tau(z_1) \simeq \frac{1}{\omega\mu_0\Delta}\left(\frac{h\Delta}{|c - z_1|^2} - \sqrt{3\varepsilon}\right),$$

$$\tau \simeq \frac{3\sqrt{3\varepsilon}}{2\omega\mu_0\Delta},$$

$$\zeta \simeq z_2 - (2/3)\Delta = z_1 + \Delta/3,$$

$$\tau(z_2) \simeq \frac{\sqrt{3/\varepsilon}}{\omega\mu_0\Delta},$$

$$\lambda \simeq \frac{3\sqrt{3/\varepsilon}}{4\omega\mu_0\Delta(c - z_1)^2}.$$

When entering region C the sheet at z_2 changes from infinite to finite conductance, and a mobile sheet with steeply increasing conductance first occurs at $\zeta \simeq z_1 + \Delta/3$. At the same time, $\tau(z_1)$ decreases steeply. The approximation given above leads to

$$\Delta D(z) \simeq \begin{cases} (3/4)\sqrt{3/\varepsilon}\,\mathcal{I}m[(c - z)^2/(c - z_1)^2], & 0 \le z \le z_1, \\ 1 - 9(z - z_1)(z_2 - z)/(2\Delta^2), & z_1 < z \le \zeta, \\ 1 - 3(z_2 - z)/(2\Delta), & \zeta \le z < z_2, \\ 0, & z \ge z_2, \end{cases}$$

which is different from $D(z) = w(z)$ valid for $\varepsilon = 0$. As required, $D(z) \ge 0$, $D(\zeta) = 0$, $\overline{D}'(\zeta) = 0$, and $D(z_1^+) = D(z_2^-) = 1/\Delta$. It is remarkable that $D(z)$ is only linear in $\zeta \le z < z_2$.

Region D

The conductance $\tau(z_1)$ decreases when penetrating into region C and may even vanish if $g > h$. In this case it is necessary to switch to region D, where the extremal model consists of the mobile sheet at $z = \zeta$ and the sheet at z_2. The equation of the boundary C–D is given in Appendix B.2. The system of non-linear equations agrees with (39) to (43), except that (40) is now missing and therefore only the second compatibility equation of (44) subsists. Together with (39), it allows the computation of the model parameters τ, ζ and $\tau(z_2)$ (see Appendix B.2). Moreover, λ is again given by (45).

Finally, isolines of $\bar{\sigma}_{\min}$ for the data considered previously for $\bar{\sigma}_{\max}$ are shown in Fig. 6. As expected, $\bar{\sigma}_{\min}$ is poorly constrained by this small data set. The greatest bound with $\bar{\sigma}_{\min}(z_1, z_2) = 33.4$ mS m^{-1} can be obtained for the average conductivity between $z_1 = 275$ km and $z_2 = 1057$ km, because these limits are sufficiently above and below g (the 'centre of gravity' of induced currents), such that the conducting material cannot be concealed. The maximum value of $\bar{\sigma}_{\min}$ is of the order of the apparent conductivity $\sigma_a = 1/\rho_a = 29$ mS m^{-1}.

Data errors can be taken into account in the same way as described for $\bar{\sigma}_{\max}$, i.e. either in the linear approximation on using the Lagrangian multiplier λ or exactly by a line search on the periphery of the circle of radius s around c.

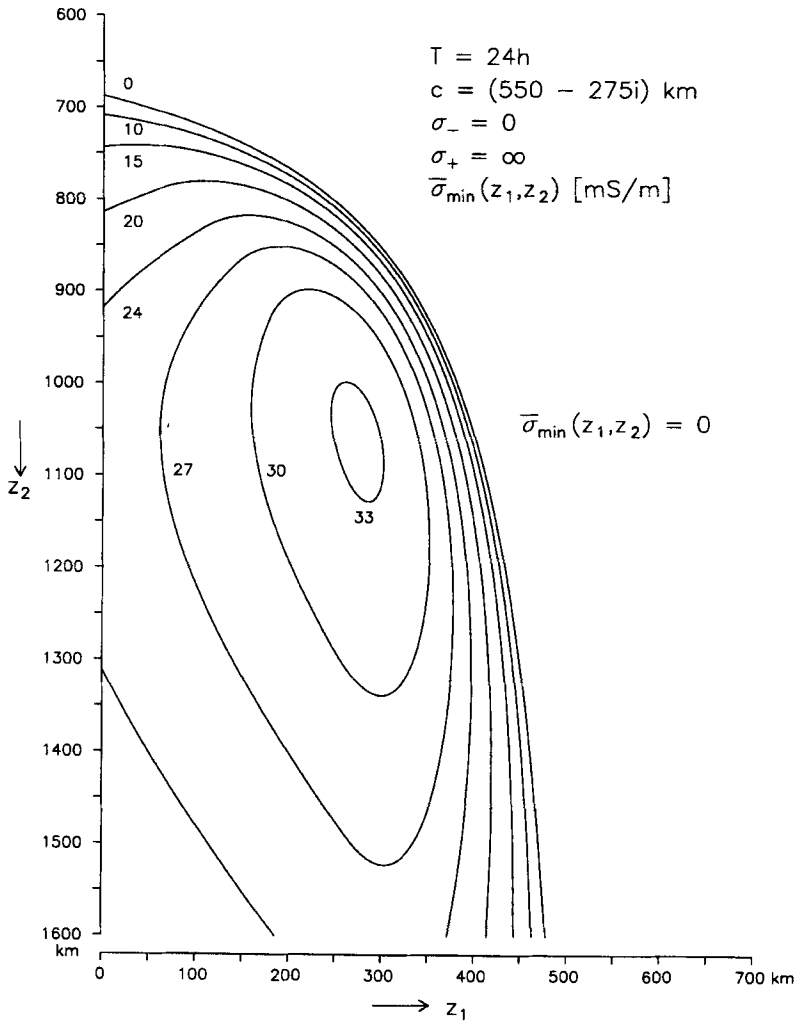

Figure 6. Isolines of $\bar{\sigma}_{min}(z_1, z_2)$ for unconstrained conductivity variations.

3.2.4 Approximate multifrequency extremal models

The one-frequency extremal models already allow an approximate treatment of the multifrequency case simply by selecting the frequency that imposes the hardest constraint on the conductivity average for a given (z_1, z_2)-range. If $\bar{\sigma}(z_1, z_2, \omega_j)$ is the average for frequency ω_j, then conservative estimates of the true extremals are defined by

$$\tilde{\bar{\sigma}}_{max}(z_1, z_2) := \min_j \bar{\sigma}_{max}(z_1, z_2, \omega_j) \geq \bar{\sigma}_{max}(z_1, z_2),$$

$$\tilde{\bar{\sigma}}_{min}(z_1, z_2) := \max_j \bar{\sigma}_{min}(z_1, z_2, \omega_j) \leq \bar{\sigma}_{min}(z_1, z_2).$$

A simple example is given in Fig. 7, which shows $\tilde{\bar{\sigma}}_{max}(z_1, z_2)$ for European average responses of the first six *Sq*-harmonics, based on the data of Olsen (1994). Each harmonic constrains the conductivity in a particular depth range (separated by dashed lines). The plot is constructed from the 1-D consistent D^+-data (Parker 1980), which essentially provide the same results as the measured data, but give a slightly clearer visualization of the depth sensitivity of the response estimates. All data are displayed in Table 1. The D^+-model has a 6.8 kS sheet at $z = 170$ km, a 61.6 kS sheet at $z = 603$ km, and an infinitely conducting sheet at $z = 695$ km. As an example, for $z_1 = 100$ km, and $z_2 = 200$ km this model leads to a conductivity average $\bar{\sigma}(z_1, z_2) = 68$ mS m^{-1}, which suggests that the conservative upper bound of 80 mS m^{-1} read from Fig. 7 is not too pessimistic.

3.3 Constrained one-frequency extremal models

3.3.1 General structure

So far $\sigma(z)$ has been allowed to vary between 0 and ∞. Now the constraints $0 < \sigma_- \leq \sigma(z) \leq \sigma_+ < \infty$ are imposed, which increases $\bar{\sigma}_{min}$ and decreases $\bar{\sigma}_{max}$. It was seen in Section 3.1 that in the one-frequency case $\sigma(z)$ only attains the values σ_- and σ_+. The bounds $\sigma_\pm$ have to be chosen sufficiently wide to warrant the existence of a model satisfying the data (see Section 3.3.2). The resulting extremal models will not then differ too much from the unconstrained case: essentially, thin sheets will be replaced by layers of finite thickness and conductivity σ_+, and insulators change into conducting layers with conductivity σ_-. Again, a layer with conductivity σ_+ lies immediately above z_2 for $\bar{\sigma}_{max}$ and immediately below that level for $\bar{\sigma}_{min}$. According to (16) $D(z) \geq 0$ for $\sigma(z) = \sigma_-$, and $D(z) \leq 0$ for $\sigma(z) = \sigma_+$.

A major qualitative change of the model structure, however, occurs at greater depth, corresponding in the unconstrained

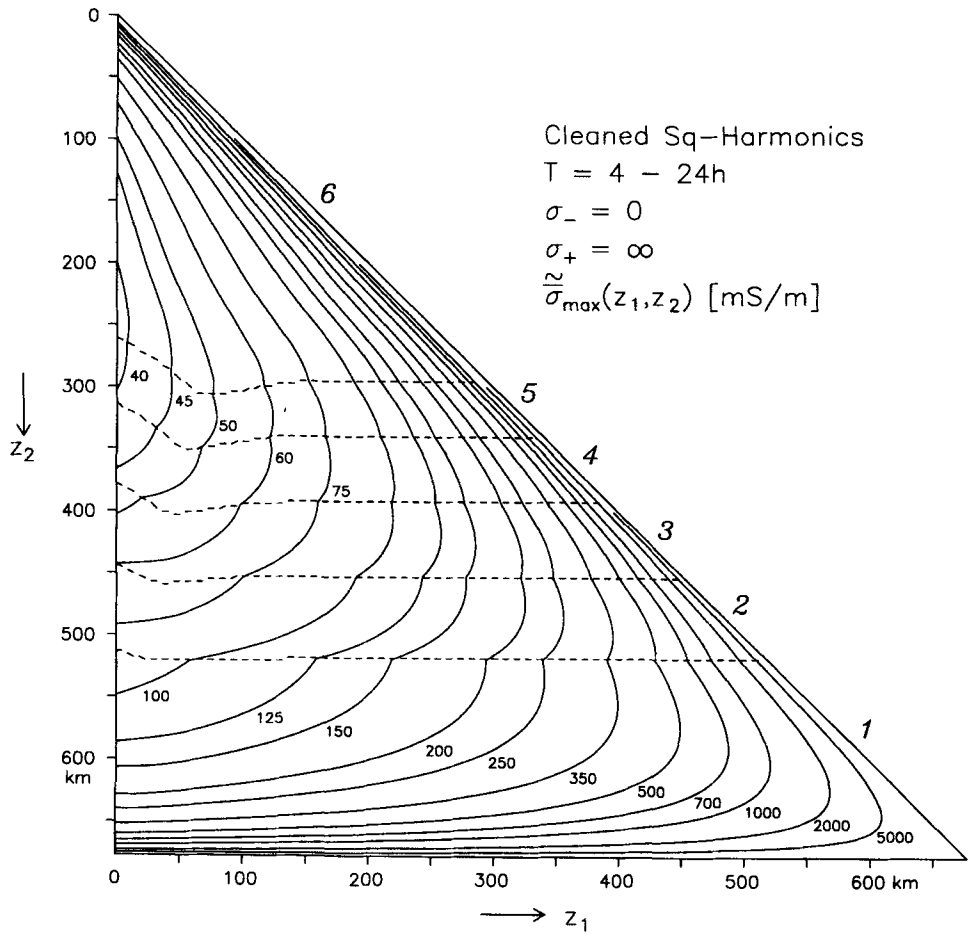

Figure 7. Isolines of the approximate multifrequency extremal $\tilde{\bar{\sigma}}_{max}(z_1, z_2)$ for European averages of the first six *Sq*-harmonics, based on the data of Olsen (1994). The dashed lines delimit the regions, in which the conductivity is constrained by the harmonics given along the diagonal.

Table 1. *c*-Responses of the first *Sq*-harmonics from Olsen (1994). The radius of the one standard deviation error circle is *s*. Fig. 7 is constructed from the 'cleaned' data (D^+-approximation).

		c(measured)		std	*c*(cleaned)	
j	*T*	*g*	*h*	*s*	*g*	*h*
	h	km	km	km	km	km
1	24	627	249	30	596	220
2	12	486	211	21	477	230
3	8	423	212	17	406	228
4	6	352	214	12	353	220
5	4.8	299	207	15	313	207
6	4	271	199	16	283	192

case to $z > \zeta_\infty$ for $\bar{\sigma}_{max}$ and $z > z_2$ for $\bar{\sigma}_{min}$. Since $E_x(z)$ performs a damped oscillation, the same applies to $F(z)$ and $D(z)$, such that all extremal models terminate with an infinite sequence of layers with alternating conductivities of σ_- and σ_+. It is now shown that the necessary extremal conditions are satisfied by a periodically layered half-space with layer thicknesses of $\pi/2$ times the local penetration depth. For this purpose let ζ_i and ζ_{i+1}, with $z_2 < \zeta_i < \zeta_{i+1}$, be the positions of two consecutive layer boundaries. Then (16) requires that

$$\mathscr{R}e[\lambda F(\zeta_i)] = 0, \qquad \mathscr{R}e[\lambda F(\zeta_{i+1})] = 0,$$

implying that $\mathscr{I}m[F(\zeta_{i+1})/F(\zeta_i)] = \mathscr{I}m[f^2(\zeta_{i+1})/f^2(\zeta_i)] = 0$. To avoid additional zeroes of $D(z)$ between ζ_i and ζ_{i+1}, we have to choose the smallest possible phase shift between $f(\zeta_i)$ and $f(\zeta_{i+1})$. Hence, $\arg[f(\zeta_{i+1})/f(\zeta_i)] = -\pi/2$. Let $k_\pm := \sqrt{i\omega\mu_0\sigma_\pm}$ and let $c_\pm$ be the response function on the top of a layer with conductivity $\sigma_\pm$ and thickness $d_\pm$. Depending on whether the conductivity between ζ_i and ζ_{i+1} is σ_- or σ_+, the field variation between the bottom and top is easily found to be

$$\frac{f(\zeta_{i+1})}{f(\zeta_i)} =: q_- = \frac{k_- + 1/c_-}{k_- + 1/c_+} \exp(-k_- d_-)$$

or

$$\frac{f(\zeta_{i+1})}{f(\zeta_i)} =: q_+ = \frac{k_+ + 1/c_+}{k_+ + 1/c_-} \exp(-k_+ d_+),$$

where periodicity demands that

$$k_- c_- = \frac{k_- c_+ + t_-}{1 + k_- c_+ t_-},$$

$$k_+ c_+ = \frac{k_+ c_- + t_+}{1 + k_+ c_- t_+},$$

$$t_\pm := \tanh(k_\pm d_\pm).$$

It is now necessary to solve these equations and $\arg q_\pm = -\pi/2$

for $d_\pm$ and $c_\pm$. The result is

$$k_- d_- = k_+ d_+ = (1+i)\pi/2 \quad \text{and} \quad c_\pm = 1/\sqrt{i\omega\mu_0\sigma_{a\pm}}, \tag{46}$$

with

$$\sigma_{a+}/\sigma_+ = \sigma_-/\sigma_{a-} = [\gamma(1-r) + \sqrt{\gamma^2(1-r)^2 + 4r}]^2/4 > 1,$$

where

$$\gamma := t_\pm = \coth(\pi/2) = 1.09033 \quad \text{and} \quad r := \sqrt{\sigma_-/\sigma_+}.$$

The layers have thickness $d_\pm = (\pi/2)p_\pm$, where $p_\pm := \sqrt{2/(\omega\mu_0\sigma_\pm)}$ is the local penetration depth.

On the top of a layer with $\sigma = \sigma_-$ or σ_+, the periodic sequence is equivalent to a *uniform* half-space with apparent conductivity σ_{a-} or σ_{a+}, which are, respectively, smaller or greater than the smallest or greatest conductivity of the constituents forming the conductor. Physically this is obvious from the fact that the periodic structure forms a sequence of quarter-wavelength plates (wavelength $2\pi p_\pm$) with a phase lag of $\pi/2$ for each traverse of a layer. At an interface, the phase lag of the upward propagating reflected field with respect to the incident field is always a multiple of π: the reflected field has twice traversed all layers above the deepest point of reflection and has undergone additional phase shifts of π at interfaces to good conductors. In particular, due to the dominant contribution of the reflection at the first interface, the reflected field is in-phase with the incident electric field at the top of a layer with $\sigma = \sigma_-$ (thus increasing $|E|$) and has a phase shift π at the top of a layer with high conductivity. Therefore $\sigma_{a-} < \sigma_-$ and $\sigma_{a+} > \sigma_+$.

3.3.2 *Data constraints*

The necessary and sufficient conditions that one-frequency data c can be interpreted by a 1-D model are $g \geq 0$, $h \geq 0$, corresponding to the phase constraints $0 \leq \varphi \leq \pi/2$. However, if c is to be interpreted by an element of the constrained conductivity set, additional conditions have to be imposed on the data. This is obvious in the extreme case $\sigma_- = \sigma_+$, which allows only uniform half-spaces and subjects c to the strict requirements that $\sigma_a = \sigma_\pm$, $\varphi = \pi/4$. The dependence of the data constraints on σ_- and σ_+ will now be investigated. For this purpose we assume exact data, select σ_- and σ_+, and determine the extremal phase values at which a constrained conductivity model no longer exists for a given σ_a. The procedure is similar to the construction of extremal conductivity averages and is outlined only briefly. The Lagrange function corresponding to (7) is

$$L[\sigma] = \varphi[\sigma] + \kappa\{\sigma_a[\sigma] - \sigma_a\} + \int_0^\infty [v_+(z)\{\sigma(z) - \sigma_+\} + v_-(z)\{\sigma_- - \sigma(z)\}]\, dz,$$

where κ and $v_\pm(z) \geq 0$ are the Lagrangian multipliers. A necessary extremal condition is that the first variation with respect to σ has to vanish, yielding from

$$\frac{\delta c}{c} = -\frac{\delta\sigma_a}{2\sigma_a} + i\delta\varphi$$

and (11) that

$$G(z) := \mathcal{I}m[F(z)/c] - 2\kappa\sigma_a\, \mathcal{R}e[F(z)/c] = v_-(z) - v_+(z).$$

$G(z)$ corresponds to the control function $D(z)$ and satisfies conditions analogous to (16). Again, $G(z)$ cannot vanish in a finite interval, because the simultaneous validity of $G(z) = 0$ and $G'(z) = 0$ would imply that $\mathcal{I}m[F'(z)/F(z)] = 0$, whereas this value is in fact $-2h(z)/|c(z)|^2 < 0$. Therefore the extremal phase models also consist of a stack of layers with alternating conductivities σ_- and σ_+, and $G(z_i) = 0$ at all internal interfaces $z = z_i$, $i = 0, 1, \ldots$, and $z_i < z_{i+1}$. Then $G(z_i) = 0$ and $G(z_{i+1}) = 0$ imply that

$$\mathcal{I}m[F(z_{i+1})/F(z_i)] = \mathcal{I}m[f^2(z_{i+1})/f^2(z_i)] = 0,$$

$i = 0, 1, \ldots$. This condition requires that $\arg[f(z_{i+1})/f(z_i)]$ is an integer multiple of $\pi/2$. Since the phase decreases with depth, this phase shift is negative, and, since two *neighbouring* zeroes are considered, $\arg[f(z_{i+1})/f(z_i)] = -\pi/2$. The previous section showed that this condition can be satisfied by a periodic sequence of quarter-wavelength plates in $z \geq z_0$. The free parameter z_0 is adjusted to yield the assigned apparent conductivity σ_a.

The construction of the extremal phase models is now obvious: since small phase values less than 45° occur *if the* conductivity decreases with depth, the minimum phase model is obtained by considering a periodic sequence of quarter-wavelength plates with σ_- in the top layer, overlain by a layer of conductivity σ_+ and variable thickness z_0, $0 \leq z_0 \leq d_+$. The response $c(z_0)$ is then given by

$$c(z_0) = \frac{1}{k_+}\frac{k_+ c_- + t}{1 + k_+ c_- t}, \qquad t := \tanh(k_+ z_0),$$

where c_- is defined by (46). Particular values are $\sigma_a(0) = \sigma_{a-} < \sigma_-$, $\sigma_a(0.5d_+) = \sigma_+$, $\sigma_a(d_+) = \sigma_{a+} > \sigma_+$, $\varphi(0) + \varphi(d_+) = 45°$, and $\varphi < 45°$ inbetween. Similarly, the maximum phase model is obtained if the conductivity increases with depth, i.e. by placing a layer with conductivity σ_- and variable thickness z_0, $0 \leq z_0 \leq d_-$ over a periodic sequence with σ_+ in the top layer. Identical extremal conditions are found when extremizing the apparent conductivity for a pre-assigned phase. Therefore the convex domains contoured in the (σ_a, φ)-plane by varying the thickness of the top layer define the data constraint areas, which are shown in Fig. 8 for various ratios σ_+/σ_- (curve parameter). The dashed vertical lines mark the under- and over-shoot areas, where the apparent conductivity is smaller than σ_- or greater than σ_+.

Adopting a slightly different point of view, a simple physical meaning can be assigned to the contours in Fig. 8: if apparent conductivity and phase are continuously monitored along a downward descent through the periodic quarter-wavelength structure, then the contours are followed in a clockwise direction. An interface is crossed whenever the phase equals 45°.

The extremal phases and apparent conductivities are very close to the extremal values encountered in a simple two-layer structure with the conductivities σ_- and σ_+. For instance, for $\sigma_+/\sigma_- = 100$ the two-layer earth yields the maximum phase 77.42°, which is only slightly smaller than the extremal phase 78.00°. Also, the maximum two-layer apparent conductivity of $1.2447\sigma_+$ is very close to the extremal value of $1.2485\sigma_+$. For $\varphi = 45°$, however, the two-layer apparent conductivities $\sigma_\pm$ differ significantly from the true extremal values of $\sigma_{a+} = 1.15\sigma_+$ and $\sigma_{a-} = 0.87\sigma_-$.

3.3.3 *Examples*

As for the unconstrained case, we again consider the diurnal *Sq*-harmonic response (see Figs 1–6), now subject to the

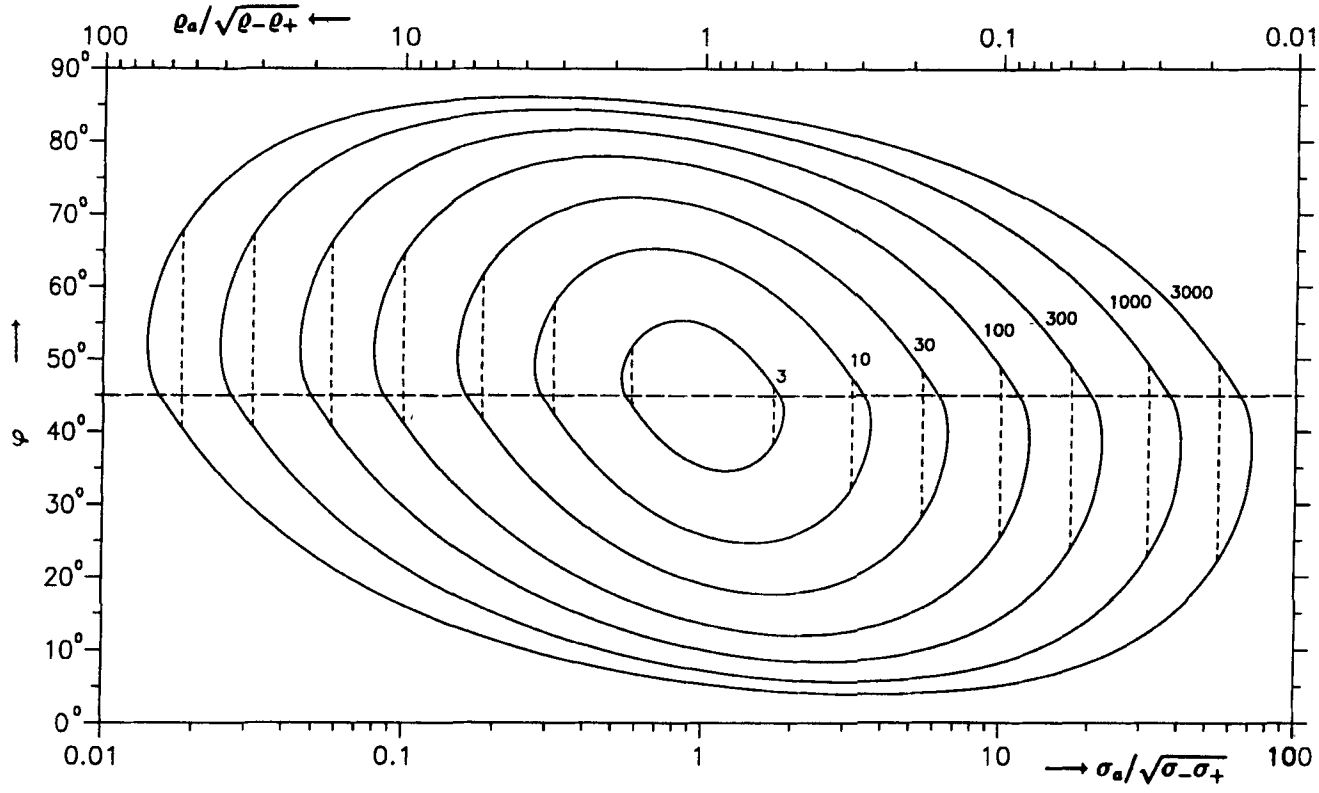

Figure 8. Joint range of apparent conductivity σ_a and phase φ for a bounded conductivity variation $\sigma_- \leq \sigma(z) \leq \sigma_+$ with σ_+/σ_- as curve parameter. The dashed vertical lines delimit under- and over-shoot areas of σ_a with $\sigma_a < \sigma_-$ and $\sigma_a > \sigma_+$.

conductivity constraints $\sigma_- = 0.01$ S m^{-1}, $\sigma_+ = 1$ S m^{-1}. Then $\sigma_a/\sqrt{\sigma_-\sigma_+} = 0.29$, $\varphi = 63°$, such that according to Fig. 8 an interpretation by a constrained conductivity model is clearly possible for $\sigma_+/\sigma_- = 100$.

First we consider the extremal models for $\bar{\sigma}_{\max}$. The required conductor configurations are shown in Fig. 9, which has to be compared with the corresponding Fig. 1 for the unconstrained case. Both figures agree on the characteristic quadruple-point topology. The finite upper bound σ_+ on the conductivity, however, leads to major changes for those pairs (z_1, z_2) for which $\bar{\sigma}_{\max}(z_1, z_2) \to \infty$ in the unconstrained case, i.e. for $z_2 \to z_{2M}$ and $z_1 \to z_2$:

(1) For $\sigma_+ = \infty$ and $z_2 \to z_{2M}$ the thin sheet at $z = z_2^-$ increases its conductance and coalesces with the perfectly conducting sheet at $z = z_{2M}$ (see Appendix B.1). A similar coalescence also occurs for $\sigma_+ < \infty$. Here the conducting layer in $z \leq z_2$ merges for large values of z_2 with the shallowest conducting $\lambda/4$-layer forming the substratum. In the present case, this occurs for $z_2 \simeq 740$ km. The electromagnetic field now penetrates the level of coalescence. This necessitates the introduction of three new conductivity configurations, which differ from the corresponding configurations at smaller z_2 by the merged substructure. The thickness of the conducting $\lambda/4$-layer is 232 km. All models obtained by a variation of z_2 in this layer clearly maximize $\bar{\sigma}(z_1, z_2)$ such that, apart from the position of z_2, the extremal models remain unchanged for 740 km $\leq z_2 \leq$ 972 km. The merging process is illustrated by means of $D(z)$ in Fig. 10(a)–(c). In the merged structure $D(z_2^-)$ is so negative that the addition of $1/\Delta$ does not change the sign.

(2) Owing to the finite value of σ_+, the thin sheet at z_2^- is replaced by a finite layer in $z \leq z_2$. For a given z_2, the thickness of the layer in $z \leq z_2$ is given by the hatched area in Fig. 9. Whenever (z_1, z_2) is in this area we obtain $\bar{\sigma}_{\max}(z_1, z_2) = \sigma_+$. In this case $\bar{\sigma}_{\max}$ is insensitive to small data changes, i.e. $\lambda = 0$ and $D(z) = w(z)$. An example is shown in Fig. 10(d). Again the necessary extremal conditions (16) are only weakly satisfied [$D(z) \leq 0$ for $\sigma(z) = \sigma_+$ and $D(z) = 0$ for $\sigma(z) = \sigma_-$].

The resulting isolines of $\bar{\sigma}_{\max}(z_1, z_2)$ are shown in Fig. 11, which should be compared with Fig. 3. The tightening of the bounds on $\bar{\sigma}(z_1, z_2)$ by imposing constraints on $\sigma(z)$ is clearly visible. The closest bound is obtained for the conductivity average between the surface and $z_2 \simeq 250$ km, which will not exceed 50 mS for any of the models satisfying this small data set.

The computation of the extremal models in the constrained case is very similar to that in the unconstrained case, although analytical solutions are no longer available. Apart from the degenerate case $D(z) = w(z)$, i.e. $\lambda = 0$, interfaces occur whenever $D(z)$ changes sign. At the discontinuities $z = z_k$, $k = 1, 2$, this requires $0 < \mathcal{R}e[\lambda F(z_k)] < 1/\Delta$. Examples considered are the computation of the quadrupole point and the level of coalescence:

Quadruple point. As can be inferred from Fig. 9, the quadruple-point model consists of four layers, with $\sigma = \sigma_-$ in $0 < z < \zeta_1$; $\sigma = \sigma_+$ in $\zeta_1 < z < z_2$; $\sigma = \sigma_-$ in $z_2 < z < \zeta_2$; and $\sigma = \sigma_{a+}$ in $z > \zeta_2$. Here $\sigma_{a+} > \sigma_+$ represents the periodic substructure (see Section 3.3.1). (In the present example $\sigma_{a+} = 1.15$ S m^{-1}.) In addition to fitting the data, the quadruple-point coordinates z_1 and z_2 with $0 < z_1 < \zeta_1$ have to be chosen in such a way that, by a small perturbation of the coordinates,

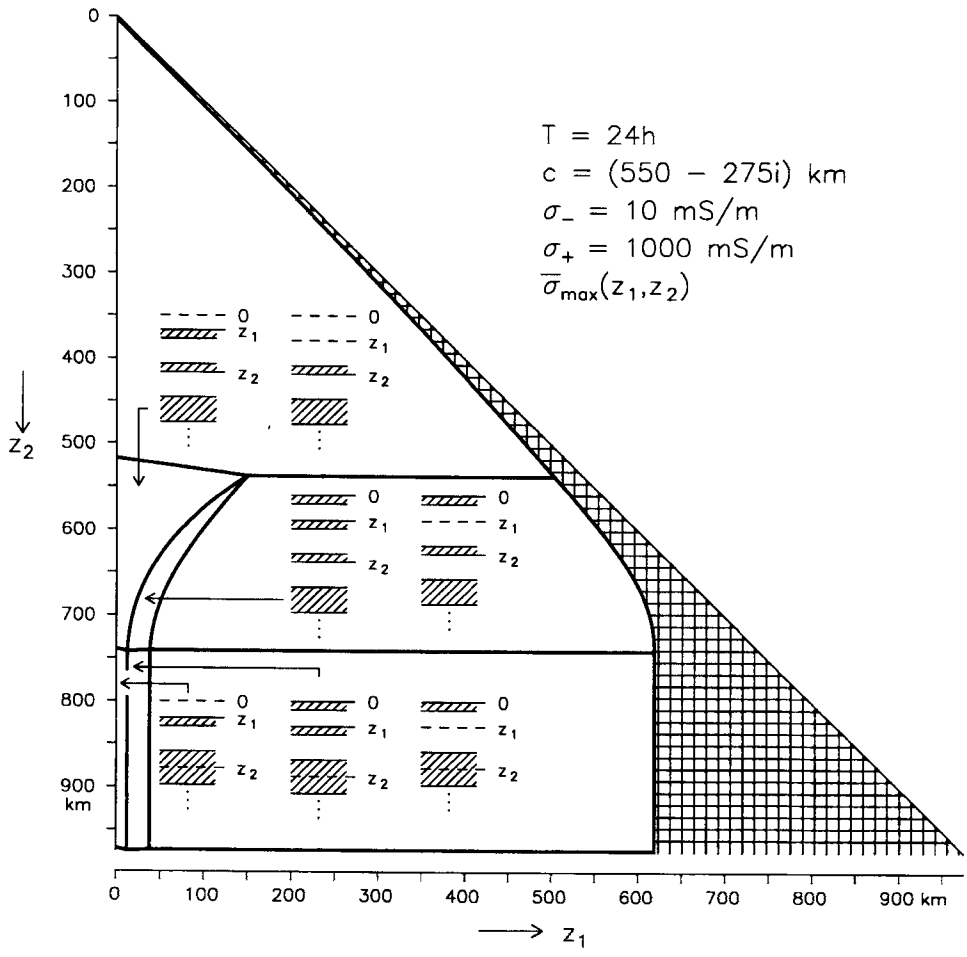

Figure 9. Structure of the constrained extremal models for $\bar{\sigma}_{\max}$. The hatched parts of the icons mark layers with $\sigma = \sigma_+$. The three dots indicate the periodicity. The deep conducting layer already belongs (fully or in part) to the periodic quarter-wavelength substructure. The poorly conducting $\lambda/4$-plate already has a thickness of 2324 km. For given z_2, the hatched area at the right marks the thickness of the conducting layer overlying $z = z_2$.

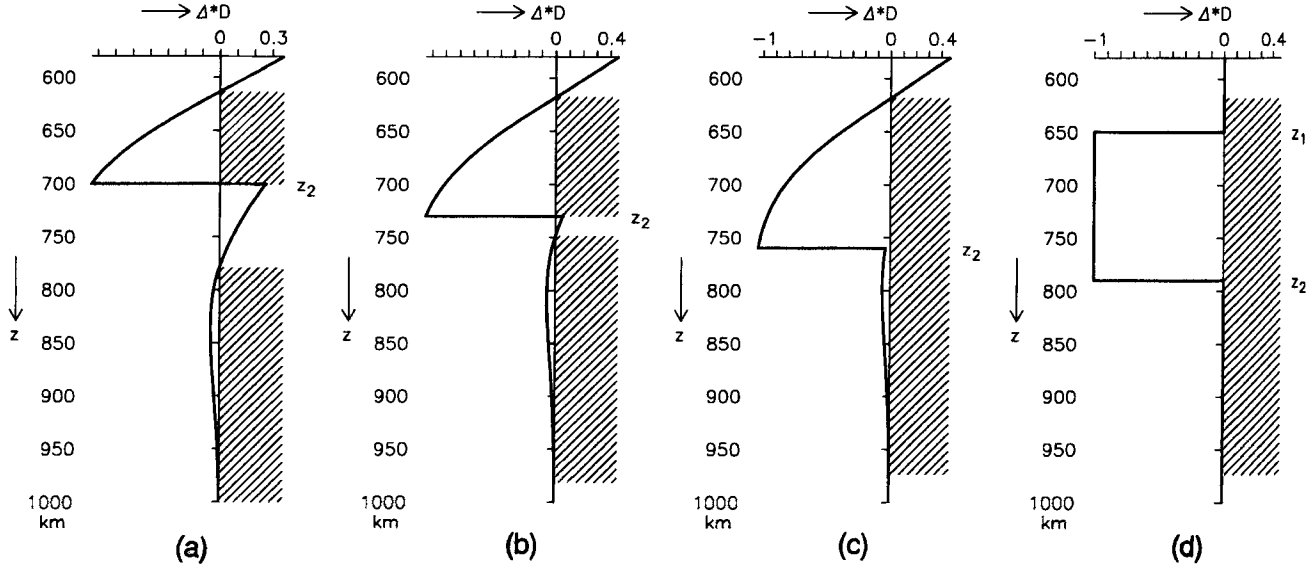

Figure 10. Typical graphs of $D(z)$ for the model of Fig. 9. Panels (a)–(c) illustrate the coalescence of the conducting layer overlying z_2 with the first conducting layer of the substratum. Panel (d) pertains to a point (z_1, z_2) of the hatched region of Fig. 9 where $D(z) = w(z)$.

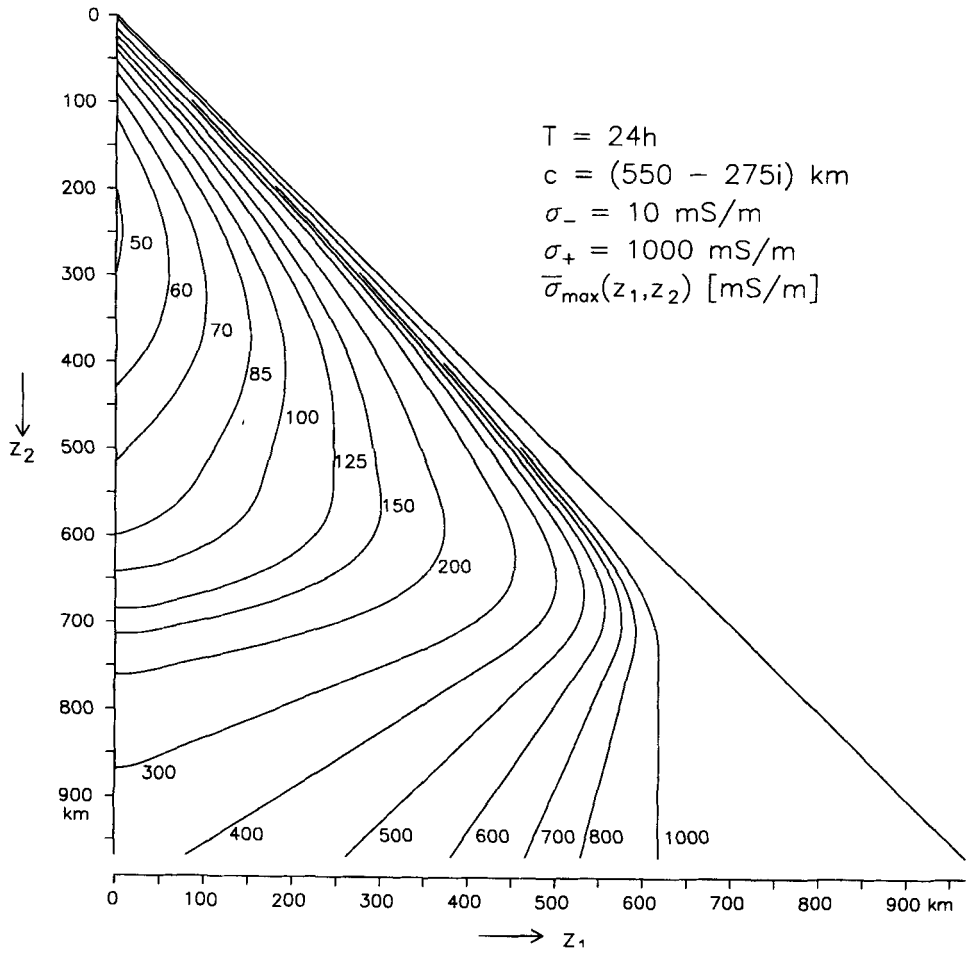

Figure 11. Isolines of $\bar{\sigma}_{\max}(z_1, z_2)$ for constrained conductivity variations.

conducting layers at $z = 0$ and/or $z = z_1$ can emerge. This leads to the conditions

$$c[\sigma] = c,$$

$$\mathcal{R}e[\lambda F(0)] = 0,$$

$$\mathcal{R}e[\lambda F(z_1)] = 1/\Delta,$$

$$\mathcal{R}e[\lambda F(\zeta_1)] = 1/\Delta,$$

$$\mathcal{R}e[\lambda F(\zeta_2)] = 0.$$

The interface depth z_2 does not enter explicitly into this system, but is implicitly taken into account when calculating $F(z)$. Hence, the above system consists of six real equations for the six real unknowns $\mathcal{R}e\,\lambda$, $\mathcal{I}m\,\lambda$, z_1, z_2, ζ_1 and ζ_2. The linear Lagrangian multiplier λ is again eliminated by the two compatibility conditions

$$\mathcal{I}m[F(\zeta_2)/F(0)] = 0, \qquad \mathcal{I}m[\{F(z_1) - F(\zeta_1)\}/F(0)] = 0,$$

which along with the first (complex) equation form a system of four non-linear equations for the four position parameters.

Level of coalescence. The determination of this is considered for the simplest case where there is a conducting surface layer only. Thus the model again consists of four layers with $\sigma = \sigma_+$ in $0 < z < \zeta_1$; $\sigma = \sigma_-$ in $\zeta_1 < z < \zeta_2$; $\sigma = \sigma_+$ in $\zeta_2 < z < z_2$; and $\sigma = \sigma_{a+}$ in $z > z_2$. The condition for coalescence at $z = z_2$ is $D(z_2^+) = 0$. Hence

$$c[\sigma] = c,$$

$$\mathcal{R}e[\lambda F(\zeta_1)] = 0,$$

$$\mathcal{R}e[\lambda F(\zeta_2)] = 1/\Delta,$$

$$\mathcal{R}e[\lambda F(z_2)] = 0.$$

Therefore the position parameters ζ_1, ζ_2 and z_2 are determined from the first equation and the compatibility condition

$$\mathcal{I}m[F(z_2)/F(\zeta_1)] = 0.$$

The solutions to the systems of non-linear equations are easily obtained by a continuous deformation of the unconstrained solution given in Appendix B.1 on using, for example, Brown's method (Brown 1973), which does not require the user to furnish the partial derivatives.

Now we briefly turn to the structure of the constrained extremal models for $\bar{\sigma}_{\min}(z_1, z_2)$, which is shown in Fig. 12. The models strongly resemble the unconstrained models (Fig. 4). A general feature is that the region in the (z_1, z_2)-plane where $\bar{\sigma}_{\min}$ exceeds σ_- has become broader (compare also Figs 6 and 13). A particularly complex sequence of conductivity models is required to transform the model with the mobile layer and the layer in $z < z_1$ (corresponding to model C in Fig. 4) to the final model for $z_1 = 0$, $z_2 \simeq 580$ km

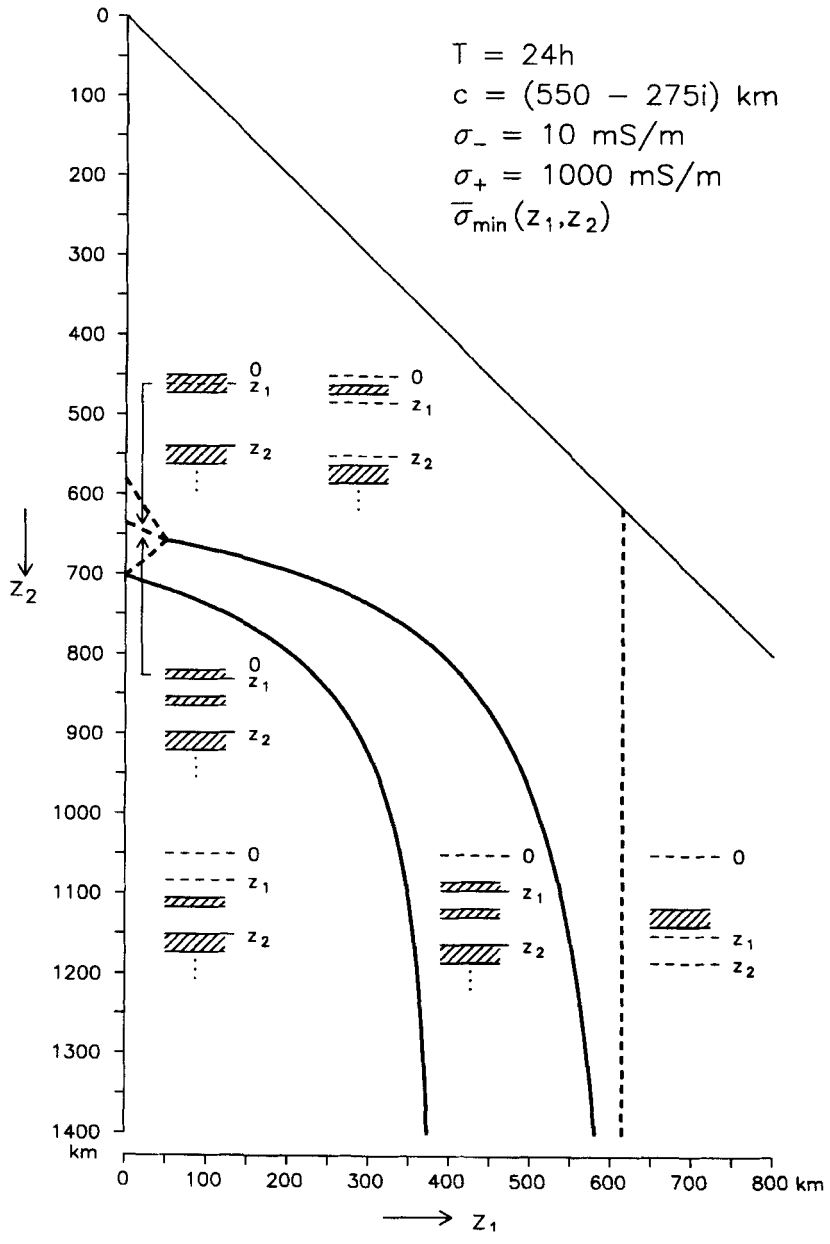

Figure 12. Structure of the *constrained* extremal models for $\bar{\sigma}_{\min}$. In contrast to Fig. 9, the deep conducting layers are thinner than $\lambda/4$ and form no part of the quarter-wavelength structure, which starts with the 2324 km thick poorly conducting layer. The model structure near $z_1 \simeq 0$, $z_2 \simeq 650$ km has been enlarged in the z_1-direction.

where the two shallow conductors are missing and $\bar{\sigma}_{\min} = \sigma_-$. The layer in $z < z_1$ touches the surface, then coalesces at $z = z_1$ with the mobile layer, and the combined conductors then gradually vanish. This sequence of events (Fig. 12) happens in the range $0 \le z_1 \le 3.2$ km only, but has been blown up for clarity. Finally, isolines of $\bar{\sigma}_{\min}(z_1, z_2)$ are displayed in Fig. 13. In comparison with Fig. 6 they show the desired increase of $\bar{\sigma}_{\min}$. $\bar{\sigma}_{\min}$ is most constrained between $z_1 \simeq 400$ km and $z_2 \simeq 1050$ km, and always exceeds 53 mS.

The comparison of the isoline plots in Figs 3 and 11 for $\bar{\sigma}_{\max}$ and in Figs 6 and 13 for $\bar{\sigma}_{\min}$ shows the possible tightening of average conductivity bounds by imposing *a priori* information. Despite this improvement, one-frequency extremal models can provide only weak bounds on the underlying conductivity structure.

4 MULTIFREQUENCY EXTREMAL CONDUCTIVITY AVERAGES

4.1 Unconstrained conductivity models

4.1.1 A two-frequency example

The extremal models for one frequency switched between the extremal conductivities σ_- and σ_+. In the multifrequency case ($M > 1$), this simple structure will also prevail, but the existence of continuous conductivity transitions can no longer be ruled out. Because of the complexity of the general case, the treatment for $M > 1$ must be confined to the presentation of partial results. First we will illustrate some of the new features through a two-frequency example.

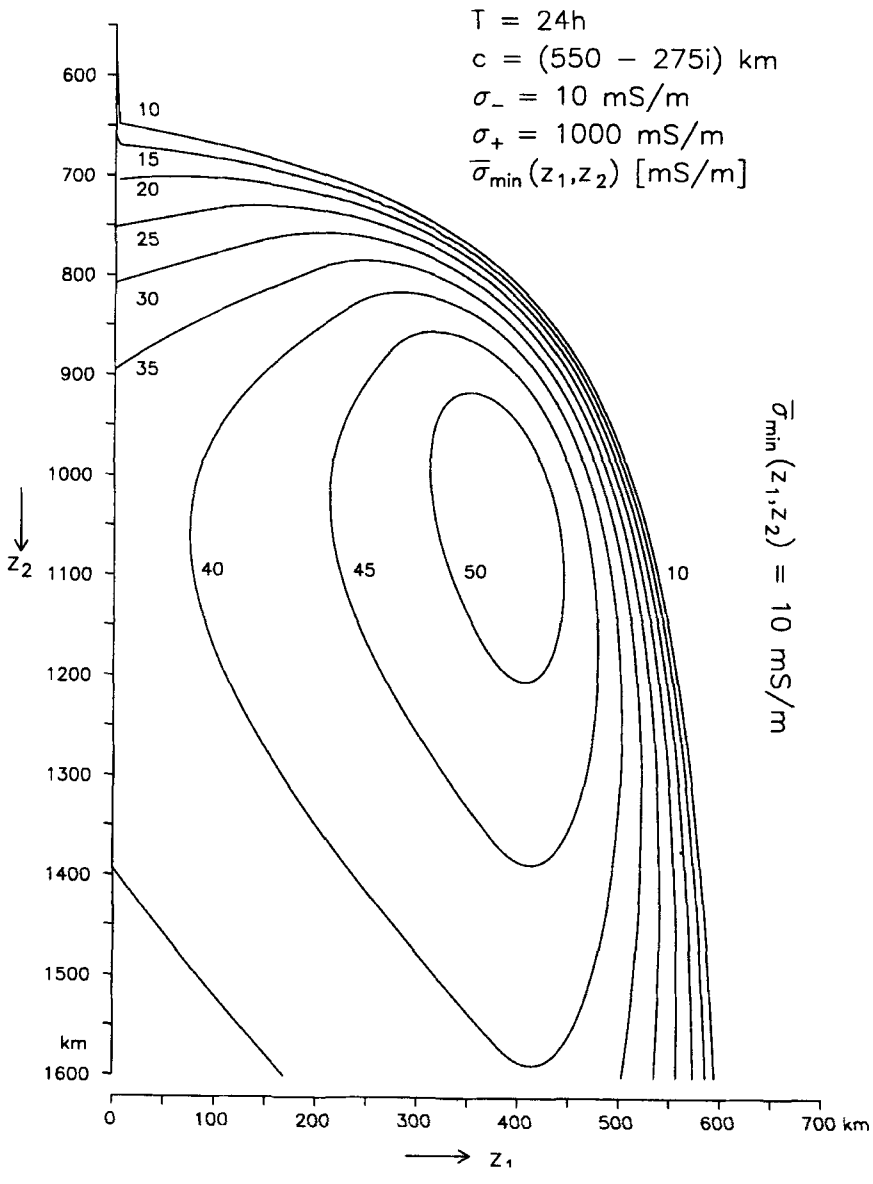

Figure 13. Isolines of $\bar{\sigma}_{\min}(z_1, z_2)$ for constrained conductivity variations.

Augmenting the previous one-frequency example by a shorter period, we consider the data set

$$T_1 = 24\,\text{h}, \quad c_1 = (550 - 275i)\,\text{km},$$
$$T_2 = 6\,\text{h}, \quad c_2 = (350 - 220i)\,\text{km}, \tag{47}$$

which simulate the first and fourth *Sq*-harmonics. Following Yee & Paulson (1988), it is seen when constructing the lens-shaped consistency region for the response of period T_2, given the response for period T_1, that the data are optimally consistent (and not close to degeneration, i.e. c_2 is not close to the boundary of the consistency region).

The four real data can be mapped into two four-parameter thin-sheet models, which are the thin-sheet model with the greatest surface conductance and the shallowest perfect conductor (model I),

$$\zeta_1 = 0.0\,\text{km}, \quad \tau_1 = 2592\,\text{S},$$
$$\zeta_2 = 460.3\,\text{km}, \quad \tau_2 = 33510\,\text{S},$$
$$\zeta_3 = 893.3\,\text{km}, \quad \tau_3 = \infty,$$

and the thin-sheet model exhibiting the deepest first conductor and smallest total conductance (model II),

$$\bar{\zeta}_1 = 214.7\,\text{km}, \quad \bar{\tau}_1 = 8487\,\text{S},$$
$$\bar{\zeta}_2 = 703.1\,\text{km}, \quad \bar{\tau}_2 = 58179\,\text{S} \tag{48}$$

(see Weidelt 1985; Yee & Paulson 1988).

Let us consider in some detail the structure of the extremal models for $\bar{\sigma}_{\max}(z_1, z_2)$, which is shown in Fig. 14 for all pairs (z_1, z_2). Although the increase of complexity compared with the one-frequency case (Fig. 1) is obvious, some simple properties are easily identified. Model I forms the backbone in the evolution of the models. Since it is the shallowest perfect conductor model, $\bar{\sigma}_{\max}(z_1, z_2) = \infty$ for $z_2 > \zeta_3 = 893$ km (bottom of the diagram). The level $\zeta_2 = 460$ km is also important: for two frequencies most extremal models for $\bar{\sigma}_{\max}$ show a mobile sheet at $z = \zeta$ with $\zeta > z_2$ for $z_2 < \zeta_2$ and $\zeta < z_2$ for $z_2 > \zeta_2$. At $z_2 = \zeta_2$, model I is realized for all z_1. The sequence of events for an interchange $\zeta > z_2 \to \zeta < z_2$ is as follows. The mobile sheet coalesces for $z_2 \to \zeta_2^-$ with the perfect conductor

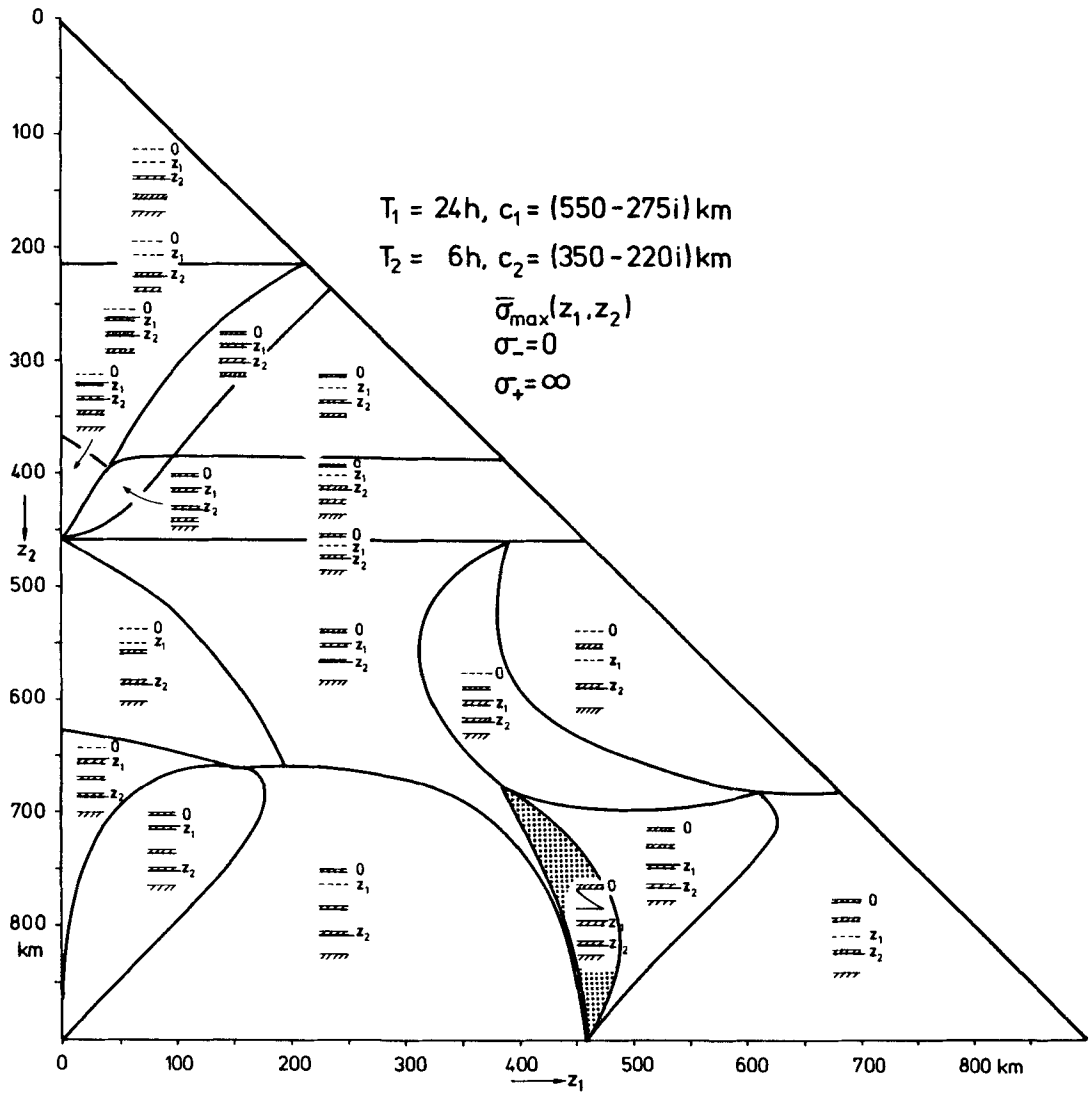

Figure 14. Structure of the extremal models $\bar{\sigma}_{max}(z_1, z_2)$ for a two-frequency problem. A continuous conductivity change is required in the shaded area.

at $z = \zeta_3^+$. Then for $z_2 > \zeta_2$ a new mobile sheet emerges in two ways: for small z_1 a sheet appears at z_1, which as z_2 increases starts moving downwards; for greater values of z_1, the surface sheet of model I becomes mobile.

The upper part $z_2 \le \zeta_2$ of Fig. 14, in common with the one-frequency case of Fig. 1, has the three-partite sequence of models with a sheet at z_1, two sheets at $z = 0$ and $z = z_1$, and only one sheet at $z = 0$. The basic difference compared with Fig. 1 is that a quadruple point Q does not occur. (It can be imagined to lie outside the triangular diagram, as also happens in the one-frequency case for $g < h$.) Moreover, the final perfect conductor disappears at $z_2 = \bar{\zeta}_1 = 214$ km (model II), but reappears for greater z_2.

The three-partite sequence also occurs in the lower part of the diagram for small z_1. The corresponding quadruple point now lies at $z_1 \simeq 150$ km, $z_2 \simeq 660$ km.

The most striking feature of Fig. 14 is the small shaded area, in which a continuous conductivity variation is required. The subsequent discussion refers to the fixed value $z_2 = 750$ km. At a mobile sheet $z = \zeta$ the control function and its average slope vanish, i.e. $D(\zeta) = 0$, $\overline{D'}(\zeta) = 0$. In general, $D'(\zeta^-) < 0$ and $D'(\zeta^+) > 0$. In exceptional situations, however, one may find that $D'(\zeta^-) = D'(\zeta^+) = 0$. This situation occurs at the right border of the shaded area for $z_1 = 468$ km. Fig. 15 shows the graph of $D(z)$ on the right (panel A). Since $D(z)$ is a quadratic function, $D(\zeta) = D'(\zeta) = 0$ and $D(0) = 0$ imply that $D(z) \equiv 0$ for $z \le \zeta$. If z_1 decreases, the slopes reverse their sign and small negative side lobes occur (panel B1 of Fig. 15), such that the first necessary condition (16) is violated. According to (27), $D(z) < 0$ indicates that $\bar{\sigma}_{max}(z_1, z_2)$ can still be *increased* by replacing the active bound $\sigma_- = 0$ by $\sigma_- > 0$ at regions with $D(z) < 0$, i.e. the model B1 for $z_1 = 446$ km is not extremal.

Therefore the extremal models for $z_1 < 468$ km are constructed by satisfying the second necessary condition of (16), $D(z) = 0$, by a continuous conductivity distribution $0 < \sigma(z) < \infty$ in $0 < z < \zeta$, where $\zeta = \zeta(z_1)$ has to be determined. Hence, for $z_1 = 446$ km the wrong model B1 in Fig. 15 is replaced by model B2 which has a continuous variation in the hatched area. Thus the sheet with $\tau = 3316$ S occurring at $\zeta = 237$ km for $z_1 = 468$ km is dissolved into a continuous profile for $z_1 < 468$ km. The hatched area gradually shrinks to zero when $z_1 = 424$ km at the left boundary of the shaded area in

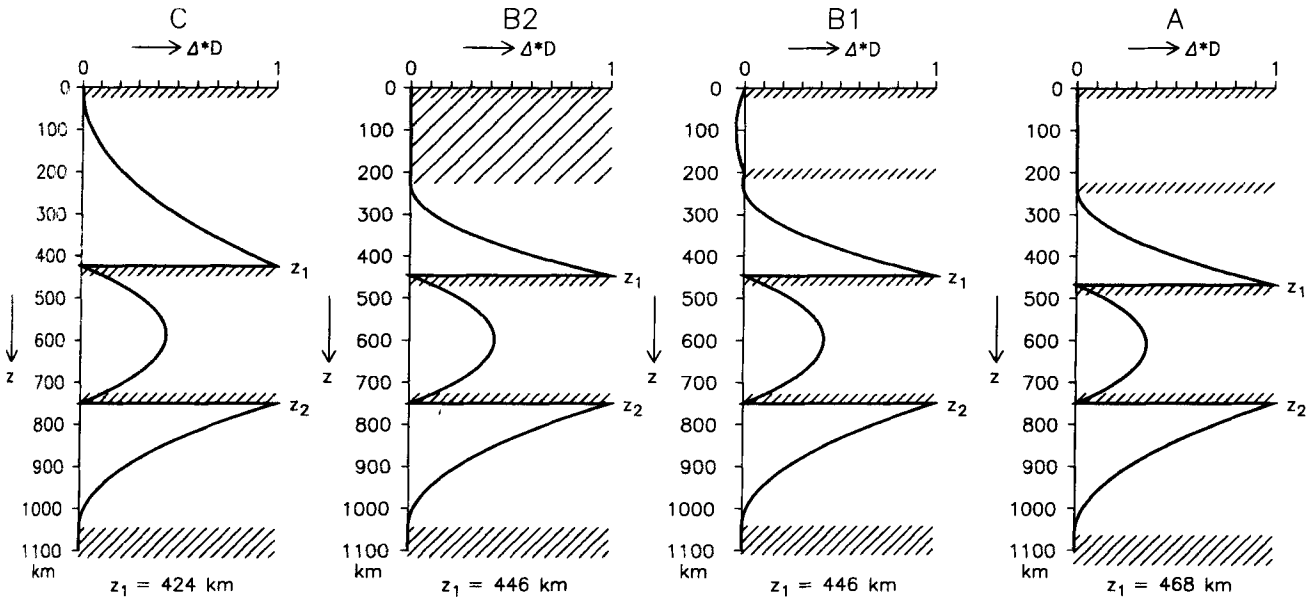

Figure 15. Typical graphs of $D(z)$ for the shaded area of Fig. 14 for variable z_1 and fixed $z_2 = 750$ km. The right boundary of the area (A) is defined by $D' = 0$ at a mobile sheet. The negative side lobes for smaller values of z_1 disqualify B1 as an extremal model. The correct model B2 shows a continuous conductivity variation in the hatched area, which gradually disappears when the left boundary is reached (C).

Fig. 14 is approached (see also panel C in Fig. 15). The resulting conductivity profiles are shown in Fig. 16 for a selection of z_1-values (curve parameter, in km).

The construction of these profiles is now briefly discussed. For this purpose (and further reference) we require the first derivatives of the Fréchet derivative $F(z)$. From (12) and (1) we obtain

$$F'' = 2i\omega\mu_0\sigma F + (F')^2/(2F), \tag{49}$$

$$F''' = 2i\omega\mu_0(2\sigma F' + \sigma' F) = 4i\omega\mu_0\sqrt{\sigma}(\sqrt{\sigma}F)', \tag{50}$$

$$F^{IV} = 2i\omega\mu_0(2\sigma F'' + 3\sigma' F' + \sigma'' F), \quad \text{etc.} \tag{51}$$

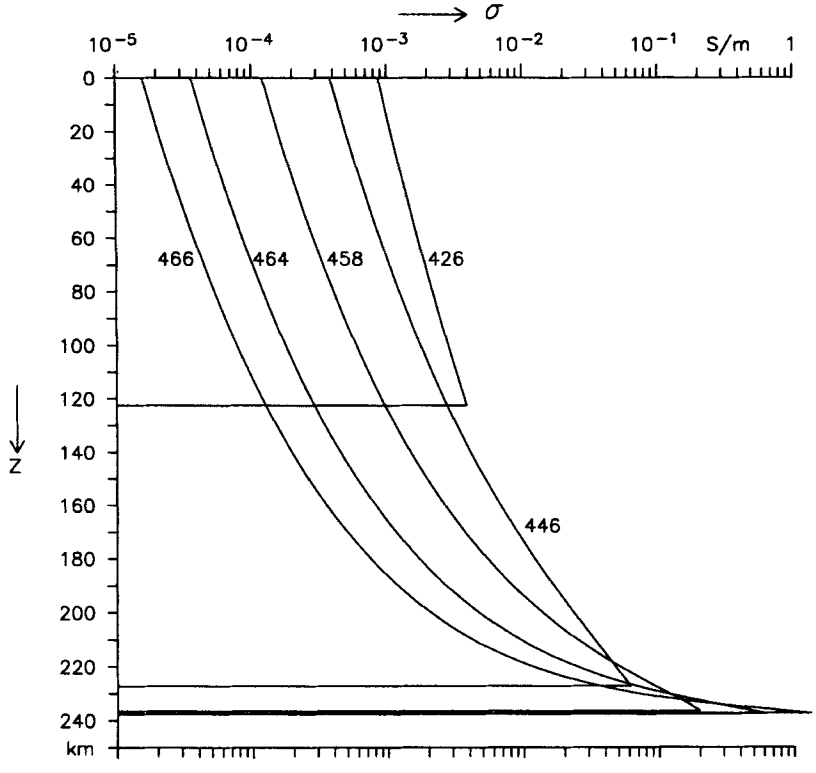

Figure 16. Conductivity variations in the shaded area of Fig. 14. The curve parameter is the value of z_1 (in km). For $z_1 = 468$ km $\sigma(z)$ is a δ-function; for $z_1 = 424$ km $\sigma(z)$ vanishes.

Eq. (50) indicates that F satisfies a *linear* third-order differential equation. Since $w(z) = 0$ for $z < z_1$, eq. (15) simplifies to

$$D(z) := \mathscr{R}e \sum_{j=1}^{2} \lambda_j F_j(z). \tag{52}$$

$D(z) \equiv 0$ implies that $D'''(z) \equiv 0$ in $0 < z < \zeta(z_1)$. Therefore (52) and (50) yield, after division by $4\mu_0\sqrt{\sigma} > 0$, integration, and squaring,

$$\sigma(z) = A \Big/ \left[\mathscr{R}e \sum_{j=1}^{2} i\omega_j \lambda_j F_j(z) \right]^2, \tag{53}$$

where A is a positive constant of integration. The definition of $\sigma(z)$ by (53) is only implicit, since $F_j(z)$ also depends (smoothly) on $\sigma(z)$. Let $\mathscr{C}^n(0, \zeta)$ be the set functions, which are n times continuously differentiable at $z \in (0, \zeta)$. If $\sigma(z) \in \mathscr{C}^n(0, \zeta)$, then (49) or (50) implies that $F_j(z) \in \mathscr{C}^{n+2}(0, \zeta)$. From (53) it follows that $\sigma(z) \in \mathscr{C}^{n+2}(0, \zeta)$, and hence that *all* derivatives of $\sigma(z)$ are continuous at $z \in (0, \zeta)$. Moreover, since $F_j(z)$ is bounded, $\sigma(z) > 0$ for $z \in (0, \zeta)$.

In the present case, the numerical task consists of the determination of the continuous function $\sigma(z)$ and of the two complex and six real discrete parameters λ_1, λ_2, A, ζ, $\tau(0)$, $\tau(z_1)$, $\tau(z_2)$ and ζ_∞. In order to do this, we can use (53) and the two complex and six real equations

$$\begin{aligned}
&c_1[\sigma] = c_1, && c_2[\sigma] = c_2,\\
&\mathscr{R}e \sum_{j=1}^{2} \lambda_j F_j(0) = 0, && \mathscr{R}e \sum_{j=1}^{2} \lambda_j F_j(\zeta) = 0,\\
&\mathscr{R}e \sum_{j=1}^{2} \lambda_j F_j'(\zeta) = 0, && \mathscr{R}e \sum_{j=1}^{2} \lambda_j F_j(z_1) = 1/\Delta,\\
&\mathscr{R}e \sum_{j=1}^{2} \lambda_j F_j(z_2) = 1/\Delta, && \mathscr{R}e \sum_{j=1}^{2} (\lambda_j/i\omega_j) F_j(z_2) = 0.
\end{aligned} \tag{54}$$

The last equation is the two-frequency analogue of (24), expressing the insensitivity of the objective function to small displacements of the final perfect conductor at $z = \zeta_\infty$. For each evaluation of an equation in the first two rows of (54), the Lagrangian multipliers λ_j are computed from the four linear equations in the last two rows and are used to obtain a self-consistent conductivity profile after a few iterative cycles of (53). With these updated values of λ_j and $\sigma(z)$, the equations in the first two rows of (54) then serve to determine the remaining six non-linear real parameters.

In the present case the construction of the correct extremal model is of mere theoretical interest, because for $z_1 = 446$ km, $z_2 = 750$ km the incorrect model B1 (Fig. 15) gives $\bar{\sigma}_{\max} = 0.263028$ S m^{-1}, which is only insignificantly smaller than the correct value of $\bar{\sigma}_{\max} = 0.263072$ S m^{-1} (model B2).

The structure of the extremal models in Fig. 14 has been obtained by gradually deforming model I, which is the firm starting point for $z_1 \to 0$, $z_2 \to 0$. The required changes of the extremal models then essentially follow from the changes of the model parameters and of $D(z)$. Typical signals for a change of the model structure are:

$\tau(z_1) \to 0^+$: omit sheet at z_1.
$D(z_1^+) \to 0^+$: include sheet at z_1.
$D(z_1^+) = 0$ and $\overline{D'}(z_1) \to 0^+$: sheet at z_1 tends to move downwards.
$\zeta \to z_1^+$: mobile sheet is fixed at z_1.
$\zeta_\infty \to \infty$: omit terminating perfect conductor.
$\zeta \to \zeta_\infty$ and $\tau \to \infty$: mobile sheet merges with terminating perfect conductor.
$D(\zeta) = 0$ and $D'(\zeta^+) \to 0^+$: introduce continuous conductor for $z < \zeta$.

The notation $D(z_1^+) \to 0^+$ etc. means that $D(z_1^+)$ tends to zero through positive values. In addition, there are analogues to the first four conditions for the surface sheet, which involve replacing z_1 by 0. The following two model changes are slightly problematic.

(1) The necessity of introducing the perfect conductor for $z_2 > 386$ km cannot be detected when the boundary is approached from above; all necessary conditions can be satisfied without this conductor also for $z_2 > 386$ km. The boundary is detected only by the diving perfect conductor when approaching it from below. This is an example where the necessary conditions (16) are not sufficient. The anomaly is connected with the fact that in both cases $D(z) \equiv 0$ below the mobile sheet.

(2) When traversing the boundary from $(z_1, z_2) = (0, 460)$ km to $(200, 660)$ km from the right, the surface sheet vanishes and the sheet at z_1 becomes mobile at the same time. This double change is required, because otherwise the model on the left would have had only three free parameters. At this boundary the continuous change of the extremal model is accompanied by a discontinuous change of $D(z)$.

In all thin-sheet cases the determination of the model parameters is simple. Consider as an example the region in Fig. 14 that is the right neighbour of the continuous conductivity region. The model parameters agree with those of that region, except that the continuous conductivity section is replaced by a thin sheet of conductance τ at $z = \zeta$. Therefore the set of necessary equations is (54) with $F_j'(\zeta)$ replaced by $\overline{F_j'}(\zeta)$. The six real equations in the first two lines form a non-linear system of equations for the determination of the six model parameters, provided that, at each call of one equation in the second line, the two complex Lagrangian multipliers λ_j are determined by solving the linear system consisting of the four real equations in the last two lines of (54).

After the detailed discussion of $\bar{\sigma}_{\max}(z_1, z_2)$, we turn our attention only briefly to $\bar{\sigma}_{\min}(z_1, z_2)$ (Fig. 17). The minimum conductance model II is a secure starting point for $z_1 \to 0$, $z_2 \to \infty$. The unexpected feature is the *discontinuous* change of the extremal models along the two barred lines. In a strip along these border lines, both models satisfy the necessary extremal conditions. The shape of the boundary is therefore found only by comparing the actual values of $\bar{\sigma}(z_1, z_2)$.

4.1.2 *General structure of the unconstrained extremal models*

The two-frequency example of the previous section, requiring a continuous conductivity layer in $0 < z < z_1$, shows that the unconstrained multifrequency extremal models in general no longer lie in the class of thin-sheet models, which is the only type we encountered for one frequency. Negative side-lobes of $D(z)$ in multifrequency thin-sheet models signal the necessity of introducing a continuous conductor. The discussion of the multifrequency case has to consider separately the structures of the extremal models in $z > z_2$ and $z < z_2$.

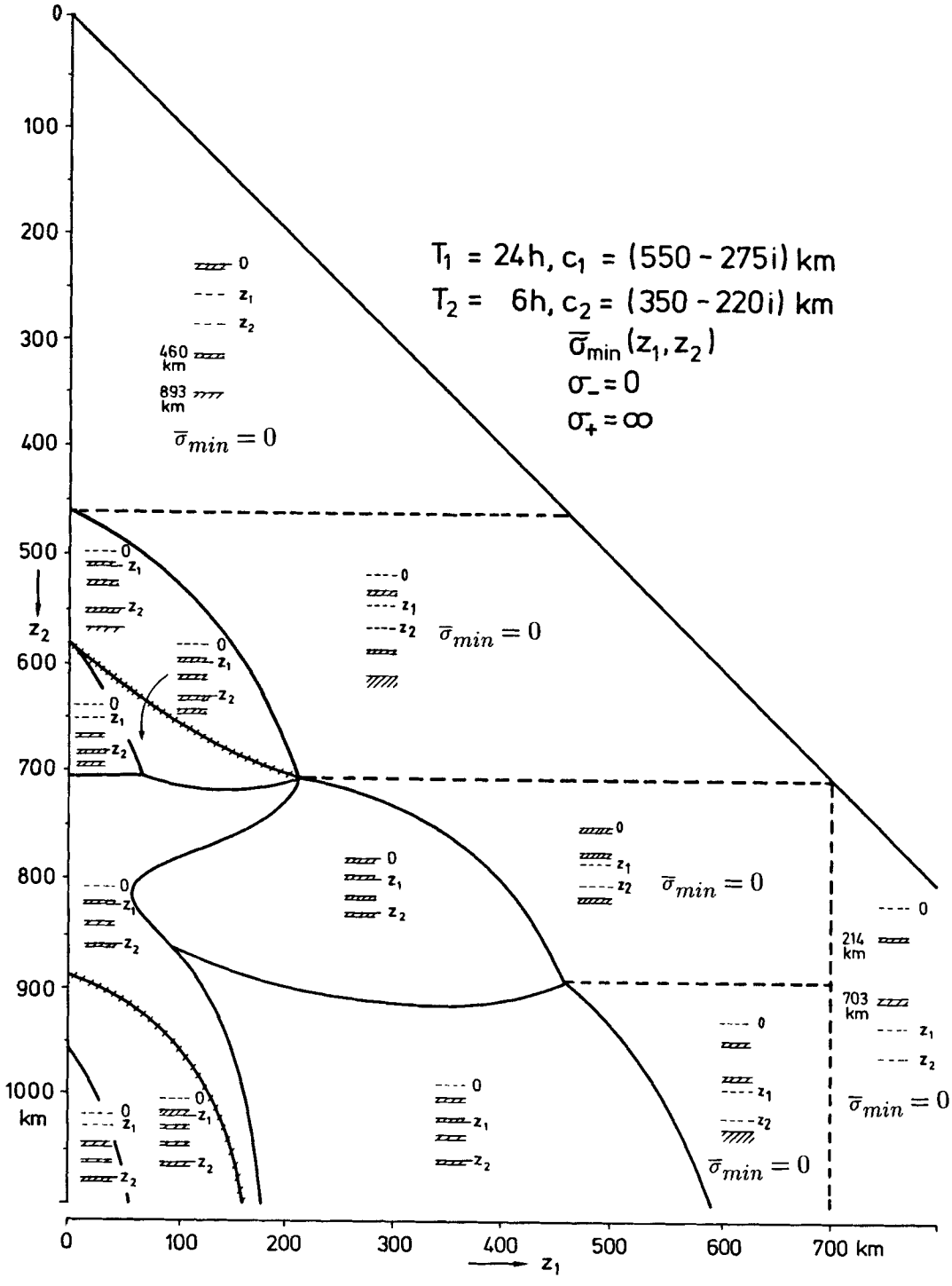

Figure 17. Structure of the extremal models $\bar{\sigma}_{\min}(z_1, z_2)$ for a two-frequency problem. A discontinuous model change occurs across the barred lines. The models giving $\bar{\sigma}_{\min}(z_1, z_2) = 0$ are non-unique.

(a) Structure in $z > z_2$

Assume first that no continuous conductivity variation exists in $z > z_2$. Then the model is terminated either by a perfect conductor at $z = \zeta_\infty$ or by an insulator, and $D(z) \to 0$ and $D'(z) \to 0$ for $z \to \zeta_\infty$ or $z \to \infty$. Between sheets, $D(z)$ varies quadratically. Let the deepest finite-conductance sheet be at $z = \zeta_n$. If it is mobile, then $D(\zeta_n) = 0$ and $\overline{D'}(\zeta_n) = 0$ imply that $D(z) \equiv 0$ for $z \geq \zeta_n$ and $D'(\zeta_n^+) = D'(\zeta_n^-) = 0$. If the adjacent sheet at $z = \zeta_{n-1}$ is also mobile, then $D(\zeta_{n-1}) = 0$ implies that $D(z) \equiv 0$ for $z \geq \zeta_{n-1}$. Continuing these arguments, we infer that $D(z) \equiv 0$ for $z \geq \zeta_1$, where ζ_1 is the position of the first sheet in $z > z_2$. For $\bar{\sigma}_{\min}(z_1, z_2)$ we have $\zeta_1 = z_2^+$. In $z > \zeta_1$, the necessary extremal condition $D(z) \geq 0$ for $\sigma(z) = 0$ can be realized only in its weak sense.

Now we have to investigate whether the thin-sheet structure can merge at some depth level ζ (e.g. immediately above a sheet) into a continuous conductivity structure, which also

requires $D(z) \equiv 0$. The results of this investigation can be summarized as follows.

(1) No continuous conductivity structure can exist in $z \geq z_2$.
(2) In $z > z_2$, at most $M-1$ mobile sheets occur, possibly terminated by a perfectly conducting sheet.
(3) A maximum number of $M-1$ mobile sheets (and a terminating perfect conductor) can occur in the extremal models for $\bar{\sigma}_{\max}(z_1, z_2)$ in the limit $z_2 \to 0$.
(4) Thin sheets are required for $\bar{\sigma}_{\max}$ at $z = z_2^-$ and for $\bar{\sigma}_{\min}$ at $z = z_2^+$.

In what follows, Propositions 1 and 2 are proved by showing that the converse assumption leads to a contradiction. In particular we try to establish, on the basis of the converse assumption, $2M$ homogeneous linear equations:

$$\mathscr{Re} \sum_{j=1}^{M} (i\omega_j)^n \Psi_j = 0, \qquad n = 0, \ldots, 2M-1, \tag{55}$$

for the complex quantities Ψ_j, which decouple into two systems of M equations for $\mathscr{Re}\,\Psi_j$ and $\omega_j \mathscr{Im}\,\Psi_j$ with the non-singular Vandermonde determinant $\det \omega_j^{2n}$ $j = 1, \ldots, M$, $n = 0, \ldots, M-1$. Hence, (55) admits only the trivial solution $\Psi_j = 0$, which will then invalidate the converse assumption.

Proof of Proposition 1

The proof essentially follows W1. Assume that $\sigma(z)$ shows a transitional variation $0 < \sigma(z) < \infty$ in $z \in (a, b)$, $a \geq z_2$, and let $\Phi_j(z) := \lambda_j F_j(z)$. Then according to (15) and (16)

$$\mathscr{Re} \sum_{j=1}^{M} \Phi_j(z) = 0, \quad \text{for } z \in (a, b). \tag{56}$$

The continuous section cannot reach to infinity, i.e. $b < \infty$. For a proof, assume the converse, differentiate (56) three times with respect to z, divide by $4\mu_0\sqrt{\sigma}$, and integrate from z to ∞. Using (50) one obtains

$$\mathscr{Re} \sum_{j=1}^{M} i\omega_j [\sqrt{\sigma(z)}\Phi_j(z) - \sqrt{\sigma(\infty)}\Phi_j(\infty)] = 0, \quad z > a. \tag{57}$$

A comparison with the Bessel function cases behaving as $\sigma(z) \sim z^m$, $-\infty < m < +\infty$, for $z \to \infty$ reveals that it is always the case that

$$\lim_{z \to \infty} \sqrt{\sigma(z)}\Phi_j(z) = 0.$$

Therefore (57) reduces to

$$\mathscr{Re} \sum_{j=1}^{M} i\omega_j \Phi_j(z) = 0, \quad z > a.$$

A $(2M-2)$-fold repetition of the same process then leads to (55) with $\Psi_j = \Phi_j(z)$. Since $|F_j(z)|$ is a continuously decaying function, $\Phi_j(z) = 0$ implies that $\lambda_j = 0$, such that the extremal conductivity averages would be independent of the data. Hence, $b < \infty$.

Now assume that $z = b < \infty$ is the lower boundary of the continuous conductivity section. In the unconstrained case, only a stack of K mobile thin sheets can exist in $z \geq b$, possibly terminated by a perfect conductor. First let $K > 0$. Then the insensitivity of the objective function Q to a small change of conductance τ_k and position ζ_k of sheet k requires that $D(\zeta_k) = 0$, $\overline{D'}(\zeta_k) = 0$, which yields, using (A9),

$$\mathscr{Re} \sum_{j=1}^{M} R_n(i\omega_j)\Phi_j(\zeta_K) = 0, \qquad n = 0, \ldots, 2K-1, \tag{58}$$

where $R_n(x)$ is a polynomial in x of exact degree n, i.e. the leading coefficient does not vanish. If $K < M$, additional $2(M-K)$ equations are generated by considering the field at $z = b$. According to the discussion after eq. (53), $\sigma(z)$ has derivatives of any order and $\sigma(b^-) > 0$. Assume that the shallowest sheet lies at $z > b$. Then the situation of Appendix A applies with $\zeta_0 = b$ and $d_1 > 0$. At $z = b$ the fields F and F' are continuous. Eqs (A10), (A12) and (51) yield

$$F(b) = R_{2K}(i\omega)F(\zeta_K), \qquad F''(b^-) = R_{2K+1}(i\omega)F(\zeta_K),$$

and more generally

$$F^{(2m)}(b^-) = R_{2K+m}(i\omega)F(\zeta_K). \tag{59}$$

Since all derivatives of $D(z)$ vanish at $z = b^-$, the system (58) can be extended to $n = 2M-1$. Because R_n is of exact degree n, it is possible to diagonalize the extended system (58) by subtracting a suitable multiple of equation n from equation $k > n$, $n = 0, \ldots, M-2$, yielding

$$\mathscr{Re} \sum_{j=1}^{M} (i\omega_j)^n \Phi_j(\zeta_K) = 0, \quad n = 0, \ldots, 2M-1.$$

Hence, $\Phi_j(\zeta_K) = 0$ and $\lambda_j = 0$. Consequently, under the above assumptions no continuous conductivity exists in $z > z_2$.

Only slight modifications are necessary to reach the same conclusion for $K = 0$ or $d_1 = 0$. For instance, if in the case $K = 0$ the infinitely conducting sheet is at $z = b$, then $F(b) = 0$, $F'(b) = 0$, but $F''(b^-) = 2i\omega\mu_0[f'(b)]^2 \neq 0$. Hence

$$F^{(2m+2)}(b^-) = R_m(i\omega)F''(b^-).$$

With $\Psi_j = \Phi_j''(b^-)$ it then follows from (55) that $\Phi_j''(b^-) = 0$, and therefore that $\lambda_j = 0$. On the other hand, assuming that the continuous section starts immediately above a sheet, i.e. $d_1 = 0$, then, in view of the remark at the end of Appendix A, eq. (59) is replaced by

$$F^{(2m+2)}(b^-) = R_{2K+m}(i\omega)F(\zeta_K).$$

Proof of Proposition 2

If there were more than $M-1$ mobile sheets below z_2, then the homogeneouss equations resulting from (58) would, via (55) with $\Psi_j = \Phi_j(\zeta_K)$, immediately lead to $\lambda_j = 0$.

Proof of Proposition 3

An exact M-frequency set is called degenerate if it results from a thin-sheet structure with less than $2M$ free parameters. In this case only one conductivity model exists. It is shown in W1 and by Yee & Paulson (1988) that exact, non-degenerate M-frequency data admit the representation

$$c(\omega_j) = \sum_{m=1}^{M} \frac{a_m}{\lambda_m + i\omega_j}, \qquad j = 1, \ldots, M,$$

$a_m > 0$, $\lambda_m > 0$, which can be interpreted in terms of a surface sheet, $M-1$ mobile sheets, and a terminating perfect conductor. The surface sheet of this model has the greatest conductance of all surface sheet models fitting the data. Therefore this model is attained by $\bar{\sigma}_{\max}$ for $z_2 \to 0$.

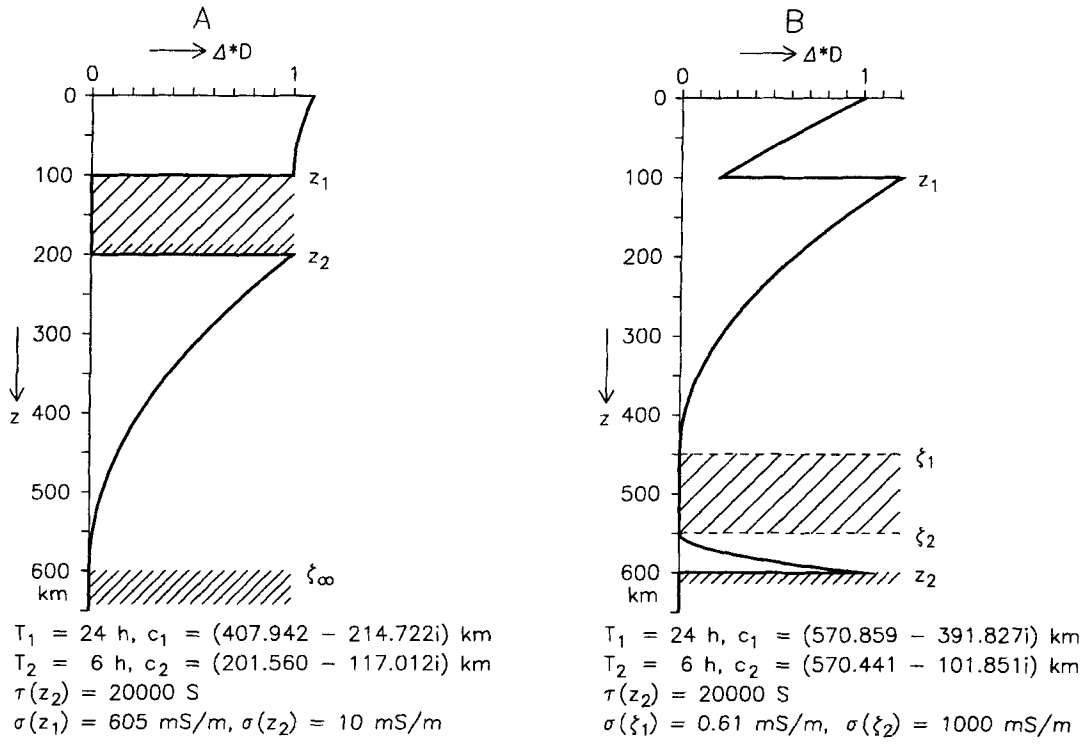

Figure 18. Two examples of extremal models with a continuous conductivity section in $z_1 < z < z_2$. A: $\bar{\sigma}_{\max}(z_1, z_2)$, B: $\bar{\sigma}_{\min}(z_1, z_2)$. The response B is dominated by the thin sheet at z_2.

Proof of Proposition 4

This has already been proved in Section 3.3 of W1.

(c) Structure in $z < z_2$

Weidelt (1985 i.e. W1) considered extremal conductance models ($z_1 = 0$) in the unconstrained case and concluded that no continuous conductivity variations could exist in $z > z_1$. However, a re-examination has shown that his conclusions are valid only for $z > z_2$ (see above), whereas—in addition to in the range $0 < z < z_1$—continuous conductivity variations can no longer be ruled out in $z_1 < z < z_2$ either. The error in W1 occurred in his eq. (A10), where the fact that $D'(z)$ is *discontinuous* across the sheet at $z = z_2$ was overlooked. In what follows, two-frequency data sets are generated which require a continuous conductivity variation also in $z_1 < z < z_2$. Two simple examples are shown in Fig. 18.

In the example for $\bar{\sigma}_{\max}(z_1, z_2)$ (A) we arbitrarily assign values to ω_1, ω_2, ζ_∞, z_2, z_1, $\tau(z_2)$ and $\sigma(z_2^-)$, then determine $\sigma(z)$ in $z_1 < z < z_2$ by satisfying all the necessary extremal conditions, and finally calculate c_1 and c_2. Once again let $\Phi_j(z) := \lambda_j F_j(z)$. The necessary extremal condition $D(z) \equiv 0$ for $z \in (z_1, z_2)$ requires in particular that $D^{(n)}(z_2^-) = 0$ for $n \geq 0$. The first four conditions are

$$\begin{aligned} &\mathcal{R}e \sum_{j=1}^{2} \Phi_j(z_2)/i\omega_j = 0, \qquad \mathcal{R}e \sum_{j=1}^{2} \Phi_j(z_2) = 1/\Delta, \\ &\mathcal{R}e \sum_{j=1}^{2} \Phi_j'(z_2^-) = 0, \qquad \mathcal{R}e \sum_{j=1}^{2} \Phi_j''(z_2^-) = 0, \end{aligned} \tag{60}$$

with

$$\begin{aligned} &\Phi'(z_2^-)/\Phi(z_2) = -2/c(z_2^-), \\ &\Phi''(z_2^-)/\Phi(z_2) = 2i\omega\mu_0\sigma(z_2^-) + 2/c^2(z_2^-), \end{aligned} \tag{61}$$

and $1/c(z_2^-) = i\omega\mu_0\tau(z_2) + 1/(\zeta_\infty - z_2)$. The four linearly independent equations can be solved for $\Phi_j(z_2)$. One possibility for the determination of $\sigma(z)$ is then a Taylor expansion at $z = z_2$, where—continuing the sequence (49) to (51)—the derivatives $\sigma^{(n)}(z_2^-)$ of the infinitely differentiable function $\sigma(z)$ are obtained from $D^{(n+2)}(z_2^-) = 0$. For instance, $D'''(z_2^-) = 0$ yields

$$\sigma'(z_2^-) = -2\sigma(z_2^-)\, \mathcal{R}e \sum_{j=1}^{2} i\omega_j \Phi_j'(z_2^-) \Big/ \mathcal{R}e \sum_{j=1}^{2} i\omega_j \Phi_j(z_2),$$

which after insertion of (61) and (60) simplifies to

$$\sigma'(z_2^-) = -4\sigma^2(z_2^-)/\tau(z_2). \tag{62}$$

The radius of convergence of the Taylor series might be very small. Therefore it is better to obtain $\sigma(z)$ implicitly by (53), which in the present context reads

$$\sigma(z) = \sigma(z_2^-) \left\{ \mathcal{R}e \sum_{j=1}^{2} i\omega_j \Phi_j(z_2) \Big/ \mathcal{R}e \sum_{j=1}^{2} i\omega_j \Phi_j(z) \right\}^2. \tag{63}$$

After a few iterative cycles starting with $\sigma(z) = \sigma(z_2^-)$, eq. (63) quickly converges to a self-consistent conductivity profile in $z_1 < z < z_2$, which can then be used to compute c_j. The approximate thin-sheet model based on this data shows thin sheets at $z_1 = 100$ km and at $\zeta = 124$ km with negative sidelobes of $D(z)$ in $z_1 < z < \zeta$ and $\zeta < z < z_2$, whereas in the true model $\sigma(z)$ decreases continuously from $\sigma(z_1^+) = 605\ \mathrm{mS\,m^{-1}}$ to $\sigma(z_2^-) = 10\ \mathrm{mS\,m^{-1}}$. Again the approximate maximum

245.097 mS m^{-1} cannot be distinguished from the true maximum $\bar{\sigma}_{\max}(z_1, z_2) = 245.115$ mS m^{-1}.

The continuous conductivity model for $\bar{\sigma}_{\min}(z_1, z_2)$ (Fig. 18, panel B) is constructed similarly. Assigning arbitrary values to ω_1, ω_2, ζ_1, ζ_2, z_2, z_1, $\tau(z_2)$ and $\sigma(\zeta_2^-)$, the first four conditions are

$$\mathscr{R}e \sum_{j=1}^{2} \Phi_j(z_2) = 0, \qquad \mathscr{R}e \sum_{j=1}^{2} \Phi_j(\zeta_2) = -1/\Delta,$$
$$\mathscr{R}e \sum_{j=1}^{2} \Phi_j'(\zeta_2) = 0, \qquad \mathscr{R}e \sum_{j=1}^{2} \Phi_j''(\zeta_2^-) = 0,$$

augmented by an equation analogous to (61) with z_2 replaced by ζ_2. Moreover, $\Phi(z_2)/\Phi(\zeta_2) = [c(z_2^-)/c(\zeta_2)]^2$, with $c(\zeta_2) = z_2 - \zeta_2 + c(z_2^-)$ and $1/c(z_2^-) = i\omega\mu_0\tau(z_2)$. The relation corresponding to (61) is $\sigma'(\zeta_2^-) = 4\sigma(\zeta_2^-)/(z_2 - \zeta_2)$. In the present example, $\sigma(z)$ increases continuously with depth. Again there is a negligible difference between the approximate and the true minimum (16.20 and 16.00 mS m^{-1}, respectively).

4.1.3 *Number of thin sheets*

Of particular interest is the number of sheets, N, that can be expected for M frequencies. A general answer to this question turns out to be difficult. An inspection of Figs 1, 4, 14 and 17 (excluding the continuous section of Fig. 14) shows that for $M = 1, 2$ this number varies between M and $M + 3$.

If we are fitting M exact responses, the extremal models must be represented by at least $2M$ free parameters. Since the omnipresent sheet at z_2 is described by only one parameter, in general at least $N = M + 1$ sheets are required. This number is reduced to $N = M$ only in the special case when z_2 coincides with a level of model II (for example eq. 48) in which the responses are represented by M thin sheets (Weidelt 1985). In Fig. 14 this situation occurs for $z_2 = \bar{\zeta}_1 = 214$ km. If no continuous conductor occurs, the upper limit appears to be $N = M + 3$: for $\bar{\sigma}_{\max}(z_1, z_2)$, $M - 1$ mobile sheets and four one-parameter sheets at $z = 0$, z_1, z_2, and ζ_∞, and, for $\bar{\sigma}_{\min}(z_1, z_2)$, M mobile sheets and up to three one-parameter sheets. However, no general proof could be obtained for this assertion. In accordance with the fact that a continuous conductivity section can be understood as an infinite sequence of thin sheets, the continuous section of B2 in Fig. 15 can be approximated by an arbitrary number of mobile thin sheets, connected, however, by small negative side lobes. Therefore in the *general* case no finite upper bound of N exists.

In the physically realistic case of noisy data considered in the next section, where the interpretation is based on a global misfit constraint, the extremal models in general will show much less structure and even the minimum of $M + 1$ sheets may not be reached.

4.1.4 *Noisy data*

So far only exact multifrequency data have been considered. However, the analysis of noisy data under the χ^2-constraint (4) requires only a few changes. The control function is now

$$D(z) := w(z) + \mathscr{R}e \sum_{j=1}^{M} \tilde{\lambda}_j F_j(z), \tag{64}$$

with $\tilde{\lambda}_j$ defined in (14). Assuming the normal case that the χ^2-bound is active, i.e. (4) is satisfied as an equality, the data induce only one (positive) Lagrangian multiplier Λ rather than M complex multipliers λ_j. For M frequencies the structure of the extremal models for noisy data will in general be simpler than that for exact data, since the resulting model will tend to approximate an exact-data case for fewer than M frequencies, which yields a greater $\bar{\sigma}_{\max}$ and a smaller $\bar{\sigma}_{\min}$ than the exact M-frequency case. If a solution has been found for one pair (z_1, z_2), a solution for other pairs will be reached by deforming the original solution and monitoring the change of $D(z)$.

The numerical procedure for noisy data is described by an example. Assume that the extremal model for $\bar{\sigma}_{\max}(z_1, z_2)$ requires three finite conductance sheets at z_1, z_2, and $\zeta > z_2$. Then the set of five necessary conditions for the determination of $\tau(z_1)$, $\tau(z_2)$, τ, ζ and Λ is

$$\sum_{j=1}^{M} |c_j - c_j[\sigma]|^2/s_j^2 = B,$$
$$\mathscr{R}e \sum_{j=1}^{M} \tilde{\lambda}_j F_j(z_1) = 1/\Delta, \qquad \mathscr{R}e \sum_{j=1}^{M} \tilde{\lambda}_j F_j(z_2) = 1/\Delta, \tag{65}$$
$$\mathscr{R}e \sum_{j=1}^{M} \tilde{\lambda}_j F_j(\zeta) = 0, \qquad \mathscr{R}e \sum_{j=1}^{M} \tilde{\lambda}_j \overline{F_j}(\zeta) = 0.$$

Using (14), let

$$\tilde{\lambda}_j := 2\Lambda\hat{\lambda}_j, \qquad \hat{\lambda}_j = (c_j - c_j[\sigma])^*/s_j^2. \tag{66}$$

Then Λ can be eliminated from all except one equation by rewriting the last four equations of (65) as

$$\mathscr{R}e \sum_{j=1}^{M} \hat{\lambda}_j[F_j(z_2) - F_j(z_1)] = 0,$$
$$\mathscr{R}e \sum_{j=1}^{M} \hat{\lambda}_j F_j(\zeta) = 0, \qquad \mathscr{R}e \sum_{j=1}^{M} \hat{\lambda}_j \overline{F_j}(\zeta) = 0, \tag{67}$$
$$\Lambda = 1 \Big/ \left[2\Delta \mathscr{R}e \sum_{j=1}^{M} \hat{\lambda}_j F_j(z_2) \right] > 0.$$

For given model parameters $\tau(z_1)$, $\tau(z_2)$, τ and ζ, the coefficients $\hat{\lambda}_j$ defined by (66) can be calculated immediately. Therefore the first equation of (65) along with the first three equations of (67) constitute a system of four non-linear equations for the determination of the model parameters. Λ then follows from the last equation of (67), and is used via (66) and (64) to obtain $D(z)$, which then may suggest further action.

4.2 Constrained conductivity models

The constrained multifrequency case will be briefly discussed via an example only. Fig. 19 shows the structure of the models of $\bar{\sigma}_{\max}(z_1, z_2)$ for the two-frequency data (47) under the constraints $\sigma_- = 0.01$ S m^{-1}, $\sigma_+ = 1$ S m^{-1}. A comparison with the unconstrained case, Fig. 14, reveals a more regular structure of the constrained models: the two-storey structure for small z_1 (induced by the two frequencies) becomes more obvious, no continuous conductor is required, and the conducting substructure cannot disappear (as in Fig. 14 for 214 km $< z_2 <$ 386 km) since $\sigma_- > 0$ always requires a layered substructure. For given z_2, the shaded region at the diagonal shows the thickness of the conductor overlying $z = z_2$, which coalesces at $z_2 \simeq 950$ km with the substructure (compared with 750 km for the longer period only; see Fig. 9). At the shallower level of $z_2 \simeq 500$ km, two layers in $z > z_2$ have already merged. The terminating dots denote a quasi-periodic sequence of layers, which soon approaches the periodic $\lambda/4$-sequence of the longer period.

A more quantitative picture of the conductivity distribution

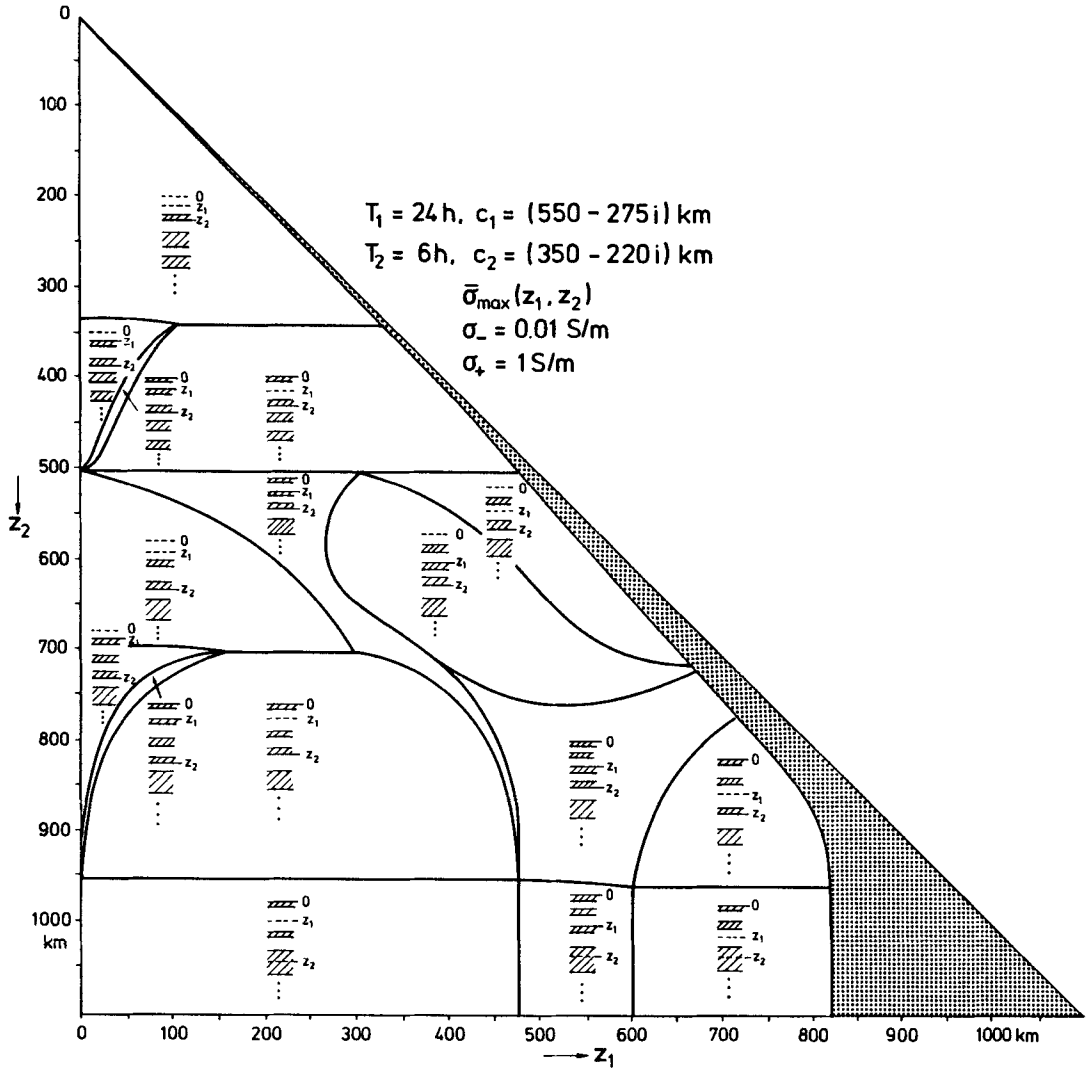

Figure 19. Structure of the constrained two-frequency extremal models $\bar{\sigma}_{max}(z_1, z_2)$. The strucure is more regular than in the unconstrained case (Fig. 14). Owing to the well-separated two frequencies, the model structure in $0 < z_2 < 500$ km is repeated below (with the mobile conducting layer now between z_1 and z_2).

for various values of z_2 is drawn in Fig. 20. For a fixed z_1 of 100 km and a varying z_2 (vertical scale), the layering in the z-direction is shown along the horizontal scale, where the conducting layers are shaded. It demonstrates nicely how, with increasing z_2, the conductor below $z = z_2$ merges with the substructure and at the same time a new conductor evolves at $z = z_1$, becomes detached, and moves downwards. This latter descent then activates a surface layer to keep the centre of gravity of induced currents at $\zeta_2^* = g_2 = 350$ km for the shorter period. At $z_2 \simeq 350$ km the conducting substructure dives down to a depth of about 2300 km and reappears for increasing z_2. This figure also illuminates the topological structure of the conducting regions in the neighbourhood of the two levels of coalescence at $z_2 \simeq 500$ km and $\simeq 950$ km.

Finally, isolines of $\bar{\sigma}_{max}(z_1, z_2)$ are displayed in Fig. 21. They show the conductivity between the surface and $z_2 = 175$ km with $\bar{\sigma}_{max} < 25$ mS m^{-1} as the best-constrained feature (compared with 40 mS m^{-1} in the absence of *a priori* conductivity bounds).

The structure of the external models in Fig. 19 has been obtained by systematically deforming the solution for small z_2 and monitoring $D(z)$. Because of the more regular structure of the constrained extremal models no problems were encountered. The following signals typically indicate that a change of model is necessary.

(1a) $\sigma(z_1^+) = \sigma_+$, $D(z_1^+) \to 0^-$: conducting layer underlying z_1 vanishes $[\sigma(z_1 + \varepsilon) = \sigma_-]$ or tends to move downwards $[\sigma(z_1 + \varepsilon) = \sigma_+]$.

(1b) $\sigma(z_1^+) = \sigma_-$, $D(z_1^+) \to 0^+$: conducting layer emerges at z_1 $[\sigma(z_1 + \varepsilon) = \sigma_-]$ or reaches z_1 from below $[\sigma(z_1 + \varepsilon) = \sigma_+]$.

(2a) $\sigma(\zeta) = \sigma_-$, $D'(\zeta) = 0$, $D(\zeta) \to 0^+$: two conducting layers coalesce at ζ.

(2b) $\sigma(\zeta) = \sigma_+$, $D'(\zeta) = 0$, $D(\zeta) \to 0^-$: conducting layer splits at ζ.

(3a) $\sigma(z_2^+) = \sigma_-$, $D(z_2^+) \to 0^+$: conducting layer overlying z_2 merges with the substructure.

(3b) $\sigma(z_2^+) = \sigma_+$, $D(z_2^+) \to 0^-$: conductor splits at z_2.

Here $\to 0^+ (\to 0^-)$ means that 0 is reached through positive (negative) values; ε is a small positive length which does not vanish in the limit under consideration. The subcases (a) and

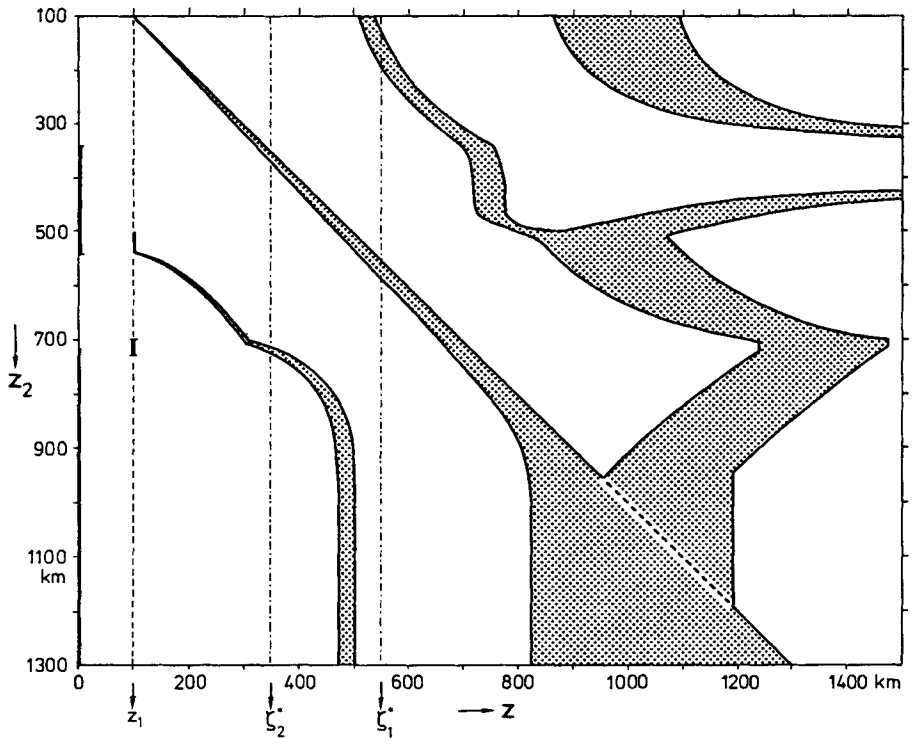

Figure 20. Quantitative structure of the extremal models $\bar{\sigma}_{\max}(z_1, z_2)$ for $z_1 = 100$ km and varying z_2 (ordinate). The horizontal axis shows the sequence of poorly and well conducting layers (shaded). The depth levels $\zeta_j^* = g_j$ mark the 'centres of gravity' of the induced currents.

(b) require inverse actions. Case 1(a,b) also holds for the surface sheet.

Although no continuous conductors were required in the simple example of Fig. 19, they will occur for other data sets and/or other *a priori* bounds. In particular, they can no longer be ruled out also in $z > z_2$. This can be anticipated from the fact that in the example, for $z_2 \simeq 500$ km, two conducting layers coalesce at $\zeta \simeq 800$ km (see Fig. 20), which requires $D(\zeta) = 0$, $D'(\zeta) = 0$ [see also case 2(a,b) above]. These are also the initial conditions for a continuous conductivity section overlying the level ζ. Therefore a different data set could require a continuous conductor also in $z > z_2$.

5 CONCLUSIONS

The scope of this paper is the investigation of how much incomplete data constrain local averages of the electrical conductivity in the simple 1-D magnetotelluric inverse problem. This task is cast into variational form and exact bounds on the average conductivity are derived in a fully non-linear treatment, at the expense of handling extended systems of non-linear algebraic equations. Therefore the exact method appears to be suitable only for data sets of modest size, whereas an approximate method (Section 3.2.4) can be applied to data sets of any size.

Layered conductors whose response is compatible with a given data set are constructed; they accomodate in a prescribed depth range $z_1 \le z \le z_2$ either as much or as little conducting material as possible. The conductivity may be constrained by *a priori* bounds $\sigma_- \le \sigma(z) \le \sigma_+$. In particular for more than one frequency, the topological structure of the extremal model is very sensitive to the depth interval $[z_1, z_2]$ (see Figs 14, 17 and 19). The control function $D(z)$ associated with the variational problem signals when changes in the model structure are necessary for varying pairs (z_1, z_2). In the unconstrained case, occasionally two competing models were found in some strip of the (z_1, z_2)-plane which both satisfied the necessary extremal conditions controlled by $D(z)$. Only by comparing the actual values of $\bar{\sigma}(z_1, z_2)$ could the true extremum be identified. Additional work is certainly required in this field.

In most cases considered, the extremal models consists of a sequence of thin sheets (or in the constrained case of a sequence of layers with alternating conductivities σ_- and σ_+). For more than one frequency, the exact extremal models may require sections with a continuous conductivity variation. However, due to the insensitivity of magnetotelluric responses to vertical conductivity gradients in the examples studied, the exact extremes could not be distinguished from the approximate bounds, where the conductivity switches between its extremes.

The isoline maps of the extremal average conductivites $\bar{\sigma}_{\max}(z_1, z_2)$ and $\bar{\sigma}_{\min}(z_1, z_2)$ for one- and two-frequency data sets simulating *Sq*-responses show, with small values for $\bar{\sigma}_{\max}$ and large values for $\bar{\sigma}_{\min}$, in which portions of the conductor the average conductivity is sensibly constrained by the data. In particular, the tightest *upper* bounds can be obtained for the conductivity average between the surface and a depth corresponding to one-half of the smallest real part of the *c*-responses used. In the *Sq*-data case, the less constrained lower bound is tightest for a conductivity average between 400 km and 1100 km, which underlines the necessity for a conductivity rise in this depth range. Although the data basis considered is very small, even two frequencies may provide useful constraints for the upper bound of the average conductivity, in particular if in addition reasonable *a priori* constraints are incorporated (Fig. 21).

The prime interest in extremal models lies not in their actual

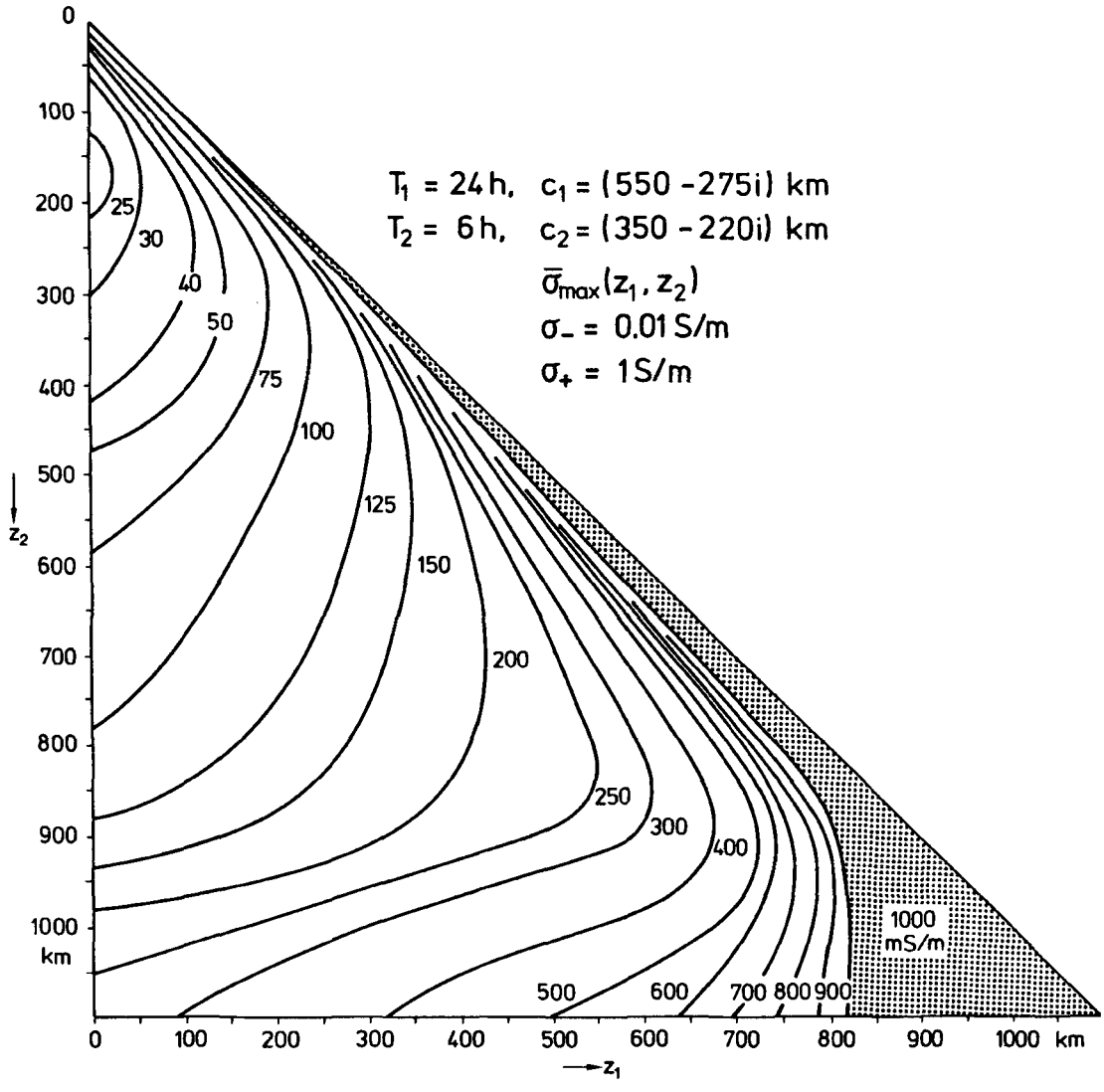

Figure 21. Isolines of $\bar{\sigma}_{max}(z_1, z_2)$ for the constrained two-frequency case. Curve labels in mS m^{-1}. In the shaded area $\bar{\sigma}_{max}(z_1, z_2) = \sigma_+$.

structure, but in the bounds they provide. However, the complexity of the problem has required an exploratory study focusing on the non-linear features of the model evolution, which even for simple data sets has revealed an unexpected dynamical behaviour.

ACKNOWLEDGMENT

The author is grateful to one of the referees for his sensible comments.

REFERENCES

Avriel, M., 1976. *Nonlinear programming, analysis and methods,* Prentice Hall, Englewood Cliffs.

Berdichevskij, M.N. & Dmitriev, V.I., 1992. *Magnetotelluric soundings of horizontally uniform media,* Nedra, Moscow (in Russian).

Brown, K.M., 1973. Computer oriented algorithm for solving systems of simultaneous nonlinear algebraic equations, in *Numerical solution of systems of nonlinear algebraic equations,* pp. 281–348, eds Byrne, G.D. & Hall, C.A., Academic Press, New York and London.

Constable, S.C., Parker, R.L. & Constable, C.G., 1987. Occam's inversion: a practical algorithm for generating smooth models from electromagnetic sounding data, *Geophysics,* **52,** 289–300.

Dosso, S.E. & Oldenburg, D.W., 1989. Linear and non-linear appraisal using extremal models of bounded variation, *Geophys. J. Int.,* **99,** 483–495.

Oldenburg, D.W., 1983. Funnel functions in linear and non-linear appraisal, *J. geophys. Res.,* **88,** 7387–7398.

Olsen, N., 1994. Bestimmung von Dst-Eindringtiefen (0.5 cpd-1/30 cpd) mittels Z/H- und Z:Y-Methode, in *Protokoll Kolloq. 'Elektromagnetische Tiefenforschung',* pp. 66–73, eds Bahr, K. & Junge, A., Deutsche Geophysikalische Gesellschaft, Hannover.

Parker, R.L., 1974. Best bounds on density and depth from gravity data, *Geophysics,* **39,** 644–649.

Parker, R.L., 1975. The theory of ideal bodies for gravity interpretation, *Geophys. J. R. astr. Soc.,* **42,** 315–334.

Parker, R.L., 1977. The Fréchet derivative for the one-dimensional electromagnetic induction problem, *Geophys. J. R. astr. Soc.,* **49,** 543–547.

Parker, R.L., 1980. The inverse problem of electromagnetic induction: Existence and construction of solutions based on incomplete data, *J. Geophys. Res.,* **85,** 4421–4428.

Schmucker, U., 1970. Anomalies of geomagnetic variations in the southwestern United States, *Bull. Scripps. Inst. Ocean. Univ. Calif.,* **13,** 1–165.

Smith, J.T. & Booker, J.R., 1988. Magnetotelluric inversion for minimum structure, *Geophysics*, **53**, 1565–1576.
Smith, R.A., 1959. Some depth formulae for local magnetic and gravity anomalies, *Geophys. Prospect.*, **7**, 55–63.
Smith, R.A., 1960. Some formulae for interpreting local gravity anomalies, *Geophys. Prospect.*, **8**, 607–613.
Weidelt, P., 1985. Construction of conductance bounds from magnetotelluric impedances, *J. Geophys.*, **57**, 191–206 (W1).
Yee, E. & Paulson, K.V., 1988. Necessary and sufficient conditions for the existence of a solution to the one-dimensional magnetotelluric inverse problem, *Geophys. J.*, **93**, 279–293.

APPENDIX A: COLLECTION OF FORMULAE FOR STACKS OF THIN SHEETS

Consider, as in Section 3.2.1, a conductivity model consisting below a level $z=\zeta_0$ of a stack of K thin sheets of finite conductance τ_k at depth $z=\zeta_k>\zeta_{k-1}$,

$$\sigma(z)=\sum_{k=1}^{K}\tau_k\delta(z-\zeta_k), \tag{A1}$$

terminated possibly by an additional perfectly conducting sheet at ζ_{K+1}. The inter-sheet separations are $d_k:=\zeta_k-\zeta_{k-1}$, $k=1,\ldots,K+1$. The integration of (1) across ζ_k using (A1) yields the jump relation (18):

$$f'(\zeta_k^+)-f'(\zeta_k^-)=i\omega\mu_0\tau_k f(\zeta_k). \tag{A2}$$

Let $f_k:=f(\zeta_k)$. Since according to (1) and (A1) $f(z)$ varies linearly between sheets, (A2) reads explicitly

$$\frac{f_{k+1}-f_k}{d_{k+1}}-\frac{f_k-f_{k-1}}{d_k}=i\omega\mu_0\tau_k f_k. \tag{A3}$$

Let

$$c_k^+=-\frac{f_k d_{k+1}}{f_{k+1}-f_k},\qquad c_k^-=-\frac{f_k d_k}{f_k-f_{k-1}} \tag{A4}$$

be the values of the response function c below and above sheet k. Then (A3) and (A4) yield, as cross-sheet and inter-sheet variations of c,

$$1/c_k^-=1/c_k^++i\omega\mu_0\tau_k, \tag{A5}$$

$$c_k^+=c_{k+1}^-+d_{k+1}, \tag{A6}$$

leading to the recursion

$$\frac{1}{c_k^-}=i\omega\mu_0\tau_k+\frac{1}{c_{k+1}^-+d_{k+1}},\qquad k=K,\ldots,1$$

starting with $c_{K+1}^-=0$. If the perfectly conducting sheet is missing, $d_{K+1}=\infty$.

The field change between adjacent sheets is

$$\frac{f_k}{f_{k-1}}=1-\frac{d_k}{c_{k-1}^+}=\frac{c_k^-}{c_k^-+d_k}=\frac{c_k^-}{c_{k-1}^+}. \tag{A7}$$

The multifrequency case in Section 4.1.2 requires some knowledge of the frequency dependence of $f(z)$ and the Fréchet derivative $F(z)$. From (A3) it follows that

$$f_{k-1}=(1+i\omega\mu_0\tau_k d_k)f_k+(d_k/d_{k+1})(f_k-f_{k+1}). \tag{A8}$$

According to whether the perfectly conducting sheet at $z=\zeta_{K+1}$ is present or absent, $f_{K+1}=0$ or $f_{K+1}=f_K$. In both cases, (A8) implies that f_{K-1}/f_K is a first-order polynomial in $i\omega$. Recursive application of (A8) then yields

$$f_{K-m}=R_m(i\omega)f_K,\qquad m=0,\ldots,K-1,$$

where $R_n(x)$ denotes a polynomial of exact degree n in x. The Fréchet derivative $F(z)=-i\omega\mu_0 f^2(z)$ and its averaged slope are then given by

$$F(\zeta_{K-m})=R_{2m}(i\omega)F(\zeta_K),\qquad \overline{F'}(\zeta_{K-m})=R_{2m+1}(i\omega)F(\zeta_K), \tag{A9}$$

since in

$$\overline{(f^2)'_k}=f_k\left[\frac{f_{k+1}-f_k}{d_{k+1}}+\frac{f_k-f_{k-1}}{d_k}\right]$$

the term $f_k f_{k-1}$ for $k=K-m$ equals $R_{2m+1}f_K^2$.

Section 4.1.2 also requires the frequency structure of the fields at the top of the stack at $z=\zeta_0$. First assume $d_1=\zeta_1-\zeta_0>0$. Then

$$F(\zeta_0)=-i\omega\mu_0 f_0^2=R_{2K}(i\omega)F(\zeta_k), \tag{A10}$$

$$F'(\zeta_0)=-2i\omega\mu_0 f_0(f_1-f_0)/d_1=R_{2K}(i\omega)F(\zeta_K), \tag{A11}$$

$$F'(\zeta_0)^2/F(\zeta_0)=-4i\omega\mu_0[(f_1-f_0)/d_1]^2=R_{2K}(i\omega)F(\zeta_K), \tag{A12}$$

where the particular structure of $R_{2K}(i\omega)$ changes from case to case. For $d_1\to 0$ we replace $(f_1-f_0)/d_1$ by (A3) for $k=1$. Then (A10) and (A11) are, respectively, polynomials of degree $2K-2$ and $2K-1$ only.

APPENDIX B: THE PARAMETERS OF THE ONE-FREQUENCY EXTREMAL MODELS

B.1 Extremal models for $\bar{\sigma}_{\max}$

The following abbreviations, which were introduced at an earlier stage, are used:

$$z_{1Q}=\frac{h|c|^2}{g(g+h)},\qquad z_{2Q}=\frac{|c|^2}{g+h},$$

$$z_{2M}=\frac{|c|^2}{g},\qquad \Delta=z_2-z_1,$$

where (z_{1Q}, z_{2Q}) are the coordinates of the quadruple point Q, z_{2M} is the depth of the shallowest perfect conductor, and Δ is the averaging range.

The boundaries $z_2=\Phi(z_1)$ between the four regions shown in Fig. 1 can be determined according to the principles stated in Section 3.2.2:

(a) Boundary A–B

$$z_2=\Phi_{AB}(z_1):=g-x,$$

where x is the positive solution of the cubic equation

$$x^3+(g-z_1)x^2+3h^2x-(g-z_1)h^2=0.$$

(The existence of only one positive solution follows from $g-z_1>0$ and Descartes' Rule.)

(b) Boundary B–C

$$z_2 = \Phi_{BC}(z_1) := z_1 + \frac{\alpha_+ + \alpha_- - \sqrt{\alpha_+(\alpha_+ - \alpha_-)}}{2(g - z_1)|c|^2},$$

where

$$\alpha_\pm = [g(g - z_1) + h(h \pm z_1)]^2.$$

(c) Boundary C–D

$$z_2 = \Phi_{CD}(z_1) := z_{2M} - z_1.$$

(d) Boundary D–A

$$z_2 = \Phi_{DA}(z_1) := z_{2Q}.$$

Then the parameters of the extremum models are as follows:

Region A $\{z_1 < z_{1Q}$ and $z_2 < \Phi_{AB}(z_1)\}$ or $\{z_1 > z_{1Q}$ and $z_2 < z_{2Q}\}$

$$\tau(z_2) = \frac{h}{\omega\mu_0|c - z_2|^2},$$

$$\zeta_\infty = z_2 + \frac{|c - z_2|^2}{g - z_2} = g + \frac{h^2}{g - z_2},$$

$$\bar{\sigma}_{max}(z_1, z_2) = \tau(z_2)/\Delta.$$

Moreover, the Lagrangian multiplier λ and the change of $\bar{\sigma}_{max}$ due to data errors are given in (29), (35), and (36).

Region B $\{z_1 < z_{1Q}$ and $\Phi_{AB}(z_1) < z_2 < \Phi_{BC}(z_1)\}$

Let

$$y := 4[1 - \Delta(g - z_1)/|c - z_1|^2]^2,$$

$$x^2 := [1 - y + \sqrt{1 + 2y}]/(2y).$$

Then

$$\tau(z_1) = \frac{1}{\omega\mu_0\Delta}\left(\frac{h\Delta}{|c - z_1|^2} - \frac{x}{1 + 2x^2}\right),$$

$$\tau(z_2) = \frac{x}{\omega\mu_0\Delta},$$

$$\zeta_\infty = z_2 + \Delta(1 + \sqrt{1 + x^2})/x^2,$$

$$\bar{\sigma}_{max}(z_1, z_2) = [\tau(z_1) + \tau(z_2)]/\Delta.$$

The compatibility condition (30) expressed in terms of the model parameters is

$$[1 + \Delta/(\zeta_\infty - z_2)]^2 - [\omega\mu_0\tau(z_2)\Delta]^2 = 1. \qquad \text{(B1)}$$

Region C $\{z_1 < z_{1Q}$ and $\Phi_{BC}(z_1) < z_2 < \Phi_{CD}(z_1)\}$

Let

$$y := 2(1 - z_1 g/|c|^2), \qquad y_1 := (z_1/\Delta)y, \qquad y_2 := (z_2/\Delta)y$$

and let x be the greater positive solution of the equation

$$(x + \sqrt{1 + x^2})^2 + y_1\sqrt{1 + x^2} - y_2(1 + 2x^2) = 0.$$

Then

$$\tau(0) = \frac{1}{\omega\mu_0}\left[\frac{h}{|c|^2} - \left(\frac{1}{z_1} - \frac{g}{|c|^2}\right)(\sqrt{1 + x^2} - x)^2\right],$$

$$\tau(z_1) = \frac{1}{\omega\mu_0\Delta}[(z_2/z_1)(\sqrt{1 + x^2} - x)^2 + x - \sqrt{1 + x^2}],$$

$$\tau(z_2) = \frac{x}{\omega\mu_0\Delta},$$

$$\zeta_\infty = z_2 + \Delta(1 + \sqrt{1 + x^2})/x^2,$$

$$\bar{\sigma}_{max}(z_1, z_2) = [\tau(z_1) + \tau(z_2)]/\Delta.$$

The formally identical expressions in regions B and C for $\tau(z_2)$ and ζ_∞ are a consequence of the validity of (B1) in both regions.

Region D $\{z_1 < z_{1Q}$ and $\Phi_{CD}(z_1) < z_2 < z_{2M}\}$ or $\{z_1 > z_{1Q}$ and $z_{2Q} < z_2 < z_{2M}\}$

The parameters are

$$\tau(0) = \frac{1}{\omega\mu_0}\left(\frac{1}{z_{2Q}} - \frac{1}{z_2}\right),$$

$$\tau(z_2) = \frac{1}{2\omega\mu_0 z_2(1 - z_2/z_{2M})},$$

$$\zeta_\infty = \frac{z_2 z_{2M}}{2z_2 - z_{2M}},$$

$$\bar{\sigma}_{max}(z_1, z_2) = \tau(z_2)/\Delta.$$

If data errors are taken into account, $\bar{\sigma}_{max}$ varies in the limits

$$\frac{|c|^2 - s^2}{|c|^2 - s^2 - z_2(g - s)} \le 2\omega\mu_0 z_2\Delta\bar{\sigma}_{max} \le \frac{|c|^2 - s^2}{|c|^2 - s^2 - z_2(g + s)}.$$

This corresponds to (36) for Region A.

B.2 Extremal models for $\bar{\sigma}_{min}$

The boundaries $z_2 = \varphi(z_1)$ between the four regions shown in Fig. 4 can be determined according to explanations given in Section 3.2.3.

(a) Boundary A–B

$$z_1 = g.$$

(b) Boundary B–C

$$z_2 = \varphi_{BC}(z_1) := g + \frac{h^2}{g - z_1}.$$

(c) Boundary C–D

Let $y := [g - z_1 + \sqrt{(g - z_1)^2 - h^2}]/h$ with $y \to 1^+$ for $z_1 \to g - h$. Then

$$z_2 = \varphi_{CD}(z_1) := g + \frac{8y^3 h}{(y^2 - 1)(3y^2 + 1)}.$$

Region A $\{z_1 > g\}$ *and Region B* $\{z_1 < g$ and $z_2 < \varphi_{BC}(z_1)\}$

$$\bar{\sigma}_{min}(z_1, z_2) = 0.$$

The mobile intermediate sheet has conductance τ and lies at

depth ζ. Then the parameters of the extremum models yielding $\bar{\sigma}_{\min}(z_1, z_2) > 0$ are as follows.

Region C $\{\max(0, g-h) < z_1 < g$ and $z_2 > \varphi_{BC}(z_1)\}$ or $\{0 < z_1 < g-h$ and $\varphi_{BC}(z_1) < z_2 < \varphi_{CD}(z_1)\}$

Let

$$y := (g - z_1)\Delta / |c - z_1|^2,$$

$$x := (2y - 1 + \sqrt{y^2 - y + 1})/(3y).$$

Then

$$\tau(z_1) = \frac{1}{\omega\mu_0\Delta}\left(\frac{h\Delta}{|c-z_1|^2} - \frac{\sqrt{3x^2-2x}}{(1-x)(3x-1)}\right),$$

$$\tau = \frac{1}{\omega\mu_0\Delta}\frac{\sqrt{3x^2-2x}}{x(1-x)},$$

$$\zeta = z_2 - x\Delta,$$

$$\tau(z_2) = \frac{1}{\omega\mu_0\Delta\sqrt{3x^2-2x}},$$

$$\bar{\sigma}_{\min}(z_1, z_2) = \tau/\Delta.$$

The compatibility condition resulting from $\mathcal{I}m[\overline{F}(\zeta)/F(z_2)] = 0$ is

$$\tau + 2\tau(z_2) = [\omega\mu_0\tau(z_2)(z_2 - \zeta)]^2\tau. \tag{B2}$$

Region D $\{0 < z_1 < g - h$ and $z_2 > \varphi_{CD}(z_1)\}$

This region is reached only for $g > h$. Let $y := |c - z_2|^2/h^2$, $1 < y < \infty$ and let x be the *positive* solution of

$$1 + yx^2 = 2\sqrt{1 + 2x + 2x^2}.$$

The existence of this solution is easily verified by a graphical display of both sides. Moreover, $1/\sqrt{y} < x < (1 + \sqrt{1+3y})/y$. Then

$$\tau = \frac{x(3 + 2x - yx^2)}{\omega\mu_0 h(yx^2 - 1)},$$

$$\zeta = z_2 - \frac{2(z_2 - g)}{3 + 2x - yx^2},$$

$$\tau(z_2) = \frac{x}{\omega\mu_0 h},$$

$$\bar{\sigma}_{\min}(z_1, z_2) = \tau/\Delta.$$

(B2) also holds in Region D.